the plant journal

SEB Society for Experimental Biology

The Plant Journal (2014) **77,** 817–837 doi: 10.1111/tpj.12442

FEATURED ARTICLE

An integrated analysis of plant and bacterial gene expression in symbiotic root nodules using laser-capture microdissection coupled to RNA sequencing

Brice Roux[1,2], Nathalie Rodde[1,2], Marie-Françoise Jardinaud[1,2,3], Ton Timmers[1,2], Laurent Sauviac[1,2], Ludovic Cottret[1,2], Sébastien Carrère[1,2], Erika Sallet[1,2], Emmanuel Courcelle[1,2], Sandra Moreau[1,2], Frédéric Debellé[1,2], Delphine Capela[1,2], Fernanda de Carvalho-Niebel[1,2], Jérôme Gouzy[1,2], Claude Bruand[1,2] and Pascal Gamas[1,2,*]

[1]*INRA, Laboratoire des Interactions Plantes-Microorganismes (LIPM), UMR441, Castanet-Tolosan F-31326, France,*
[2]*CNRS, Laboratoire des Interactions Plantes-Microorganismes (LIPM), UMR2594, Castanet-Tolosan F-31326, France, and*
[3]*INPT-Université de Toulouse, ENSAT, Avenue de l'Agrobiopole, Auzeville-Tolosane, Castanet-Tolosan F-31326, France*

Received 6 December 2013; accepted 2 January 2014; published online 31 January 2014.
*For correspondence (e-mail Pascal.Gamas@toulouse.inra.fr).
Accession number for raw RNA-seq data: SRP028599 (Sequence Read Archive, SRA)

SUMMARY

Rhizobium-induced root nodules are specialized organs for symbiotic nitrogen fixation. Indeterminate-type nodules are formed from an apical meristem and exhibit a spatial zonation which corresponds to successive developmental stages. To get a dynamic and integrated view of plant and bacterial gene expression associated with nodule development, we used a sensitive and comprehensive approach based upon oriented high-depth RNA sequencing coupled to laser microdissection of nodule regions. This study, focused on the association between the model legume *Medicago truncatula* and its symbiont *Sinorhizobium meliloti*, led to the production of 942 million sequencing read pairs that were unambiguously mapped on plant and bacterial genomes. Bioinformatic and statistical analyses enabled in-depth comparison, at a whole-genome level, of gene expression in specific nodule zones. Previously characterized symbiotic genes displayed the expected spatial pattern of expression, thus validating the robustness of our approach. We illustrate the use of this resource by examining gene expression associated with three essential elements of nodule development, namely meristem activity, cell differentiation and selected signaling processes related to bacterial Nod factors and redox status. We found that transcription factor genes essential for the control of the root apical meristem were also expressed in the nodule meristem, while the plant mRNAs most enriched in nodules compared with roots were mostly associated with zones comprising both plant and bacterial partners. The data, accessible on a dedicated website, represent a rich resource for microbiologists and plant biologists to address a variety of questions of both fundamental and applied interest.

Keywords: nitrogen-fixing symbiosis, *Sinorhizobium meliloti*, *Medicago truncatula*, model legume, transcriptome, regulators.

INTRODUCTION

Root nodules are specialized organs inside which differentiated rhizobia fix atmospheric nitrogen to the benefit of the host plant that in turn provides the bacteria with carbon resources. In addition to its agronomic and ecological importance, nodule formation represents a particularly interesting developmental program interconnecting plant and bacterial cell differentiation. It starts in the root with the exchange of specific molecular signals, involving the recognition of bacterial lipo-chito-oligosaccharidic Nod factors (NF) by LysM-type host plant receptors, leading to symbiotic responses essential for subsequent rhizobium infection and initiation of nodulation (Oldroyd *et al.*, 2011). Rhizobial infection proceeds via tubular structures originating from the plant, the infection threads (ITs); these generally form in root hairs and extend into the underlying cortical cells and into the growing nodule (Jones *et al.*,

2007; Murray, 2011). Cytokinins (CKs) play a central role in nodule initiation (Gonzalez-Rizzo *et al.*, 2006; Murray *et al.*, 2007; Tirichine *et al.*, 2007; Heckmann *et al.*, 2011), which is also dependent on auxin accumulation at defined locations (Mathesius *et al.*, 1998; Suzaki *et al.*, 2012). Cytokinins regulate several symbiosis-related transcription factors (TFs) such as NSP2, NIN and ERN1, which are essential for NF-dependent rhizobial infection and the development of mature nodules (Oldroyd and Long, 2003; Kalo *et al.*, 2005; Marsh *et al.*, 2007; Middleton *et al.*, 2007; Madsen *et al.*, 2010; Plet *et al.*, 2011; Ariel *et al.*, 2012).

Indeterminate nodules, such as those developing on roots of the model legume *Medicago truncatula,* are elongated due to the presence of an apical meristem whose activity leads to the formation of different zones representing successive developmental stages (Vasse *et al.*, 1990). Zone I (ZI) corresponds to the bacteria-free meristematic region, mostly containing non-differentiated dividing cells. Zone II (ZII), or the infection zone, comprises in its distal part non-infected differentiating cells (pre-infection zone) and cells where bacteria are released from ITs; in the proximal part of ZII, plant and bacterial cells gradually enlarge and differentiate with a series of endoreduplication cycles (Cebolla *et al.*, 1999). Zone III (ZIII) comprises symbiosomes within which nitrogen fixation by bacterial nitrogenase takes place, and which consist of differentiated bacteroids surrounded by a peribacteroid membrane of plant origin. A region a few cell layers wide, termed the interzone (IZ), has been identified between ZII and ZIII. After several weeks, a senescence zone, zone IV, gradually develops from the proximal part of the nodule (Pérez Guerra *et al.*, 2010).

Several transcriptomic studies performed on entire *M. truncatula* nodules have established that the expression of thousands of genes is affected during nodule development. Analyses of nodules harvested at various times after inoculation, or blocked at an early stage of bacteroid differentiation, made it possible to distinguish the *Sinorhizobium meliloti* bacteroid transcriptome at early and late differentiation stages (Capela *et al.*, 2006). The coordinated regulation of numerous *M. truncatula* genes has also been shown, with successive waves depending notably on bacterial infection and bacteroid differentiation (El Yahyaoui *et al.*, 2004; Mitra *et al.*, 2004; Lohar *et al.*, 2006; Van de Velde *et al.*, 2006; Godiard *et al.*, 2007; Benedito *et al.*, 2008; Maunoury *et al.*, 2010; Moreau *et al.*, 2011; Boscari *et al.*, 2013). As an example of genes revealed thanks to transcriptomic analyses, members of the large family of plant genes encoding small cysteine-rich proteins (NCRs) (Fedorova *et al.*, 2002; Mergaert *et al.*, 2003; Graham *et al.*, 2004) were shown to play essential roles during bacteroid differentiation in indeterminate nodules (Van de Velde *et al.*, 2010) but not in *Lotus japonicus* or soybean determinate-type nodules (Colebatch *et al.*, 2002, 2004; Kouchi *et al.*, 2004; Hogslund *et al.*, 2009; Libault *et al.*, 2010; Severin *et al.*, 2010). Transcriptome analyses also identified TF-encoding genes upregulated in *M. truncatula* nodules, including *MtNF-YA1* (Combier *et al.*, 2006; Laloum *et al.*, 2012), important for nodule meristem establishment or maintenance, *MtZPT2.1* and *MtEFD*, involved in the differentiation of ZII and ZIII (Frugier *et al.*, 2000; Vernié *et al.*, 2008), and *MtbHLH1*, necessary for proper vascularization and metabolic exchanges between the nodule and the rest of the plant (Godiard *et al.*, 2011).

Whole-organ analyses do not allow a precise spatio-temporal analysis of gene expression during nodule development. Laser-capture microdissection (LCM) has been successfully used in several plant species to isolate a range of cell types or tissues (see for reviews Day *et al.*, 2005; Galbraith and Birnbaum, 2006; Ramsay *et al.*, 2006; Rogers *et al.*, 2012). Coupled with *in vitro* amplification of extracted RNAs, this technique enables genome-wide analysis of gene expression in specific cells. In recent years, it has been used to characterize various plant–microbe interactions (Hogekamp *et al.*, 2011; Damiani *et al.*, 2012; Gaude *et al.*, 2012; Takanashi *et al.*, 2012; Zhang *et al.*, 2012), including *M. truncatula* nodules (Limpens *et al.*, 2013). Those studies were based on Affymetrix chip hybridizations and targeted a single (plant or microbial) partner of the interaction.

Here we report the development of a highly sensitive approach coupling LCM to RNA sequencing (RNA-seq) to decipher the concomitant transcriptome of both bacterial and plant partners in different zones of the nodule. We used oriented RNA-seq analyses that make it possible to identify the transcribed DNA strand. Validated by a set of previously characterized symbiotic genes, this strategy allowed us to generate a comprehensive and dynamic view of the plant and bacterial genes involved in nodule development and activity. It also provides an important collection of candidate genes to be further validated by functional studies. We illustrate the richness of this resource, available through a dedicated website, by analyzing gene expression associated with meristem activity, cell differentiation and selected signaling processes related to bacterial Nod factors and to the redox status.

RESULTS AND DISCUSSION

A coupled LCM–RNA-seq strategy to generate plant and bacterial expression data from different nodule zones

To obtain RNA samples enriched for both plant and bacterial transcripts, we optimized an experimental procedure (termed Ribominus-like) based on the RiboMinus® strategy (Invitrogen, http://www.invitrogen.com/) to eliminate abundant plant and bacterial rRNAs and tRNAs using biotinylated oligonucleotides. We first used non-dissected roots and nodules that, for comparison, were also used for the purification of polyadenylated eukaryotic mRNAs. Ribominus-

like or polyA+ samples were then used for oriented RNA sequencing, using a technique based on strand-specific degradation by uracyl-*N* glycosylase (Parkhomchuk *et al.*, 2009). A very high correlation was observed between the Illumina RNA-seq data from each type of preparation ($R^2 > 0.93$; Figure S1 and Table S1A in Supporting Information). Read coverage at the gene level showed an overall similar distribution, but more reads corresponded to introns in the case of Ribominus-like libraries, presumably due to the detection of unspliced non-polyadenylated mRNA precursors (see Figure S2). Importantly, the Ribominus-like technique enabled an efficient recovery of bacterial RNAs from nodule samples (Table 1). Besides, the sensitivity of the RNA-seq approach was well illustrated by the detection in root samples of a few reads for *MtENOD11*, a gene known by promoter:GUS fusion to be expressed in the root cap and lateral root primordia (Journet *et al.*, 2001), but which cannot be detected by Affymetrix chip analysis (gene probe Mtr.13473.1.S1_at; *M. truncatula* gene atlas, Noble Foundation, http://mtgea.noble.org/v3/).

This approach was then applied to laser-dissected samples from mature nodules, representing five regions (Figure 1a): the apical region with small cells, enriched for the nodule meristematic zone, termed fraction I (FI); the region below FI, collected as a distal and a proximal fraction (FIId and FIIp, respectively) and corresponding to ZII cells undergoing differentiation or infection; the interzone II–III (IZ), which separates ZII from the nitrogen-fixation zone ZIII and which can be clearly visualized by Lugol staining (Vasse *et al.*, 1990); and a large part of ZIII. Analysis of total RNA profiles from these LCM samples indicated that they differed by the relative amount of bacterial and plant rRNA (Figure 1b). As expected, bacterial rRNAs were undetectable in FI, while they gradually increased to a maximum in ZIII. Following mRNA enrichment and a single round of amplification by *in vitro* transcription, oriented paired-end sequencing was performed. Reads were mapped to the *S. meliloti* 2011 genome (Sallet *et al.*, 2013) and a new version of the *M. truncatula* A17 genome

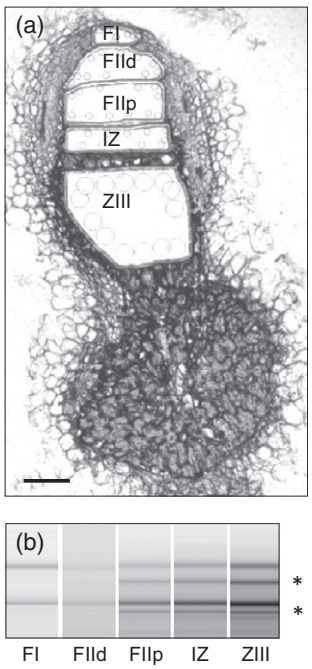

Figure 1. Laser microdissection of five regions from a 15-day-old nodule.
(a) Dissected regions.
(b) Corresponding RNA samples (asterisks, bacterial rRNAs). Scale bar: 100 μm.

Table 1 Summary of libraries and sequencing

Samples[a]	Mapped read pairs	Read pairs used for expression analyses		Non-ambiguous mapping rate, %
		Medicago truncatula	*Sinorhizobium meliloti*	
Whole roots (rbm)	152 866 480	131 328 859	12 246[b]	85.9
Whole roots (polyA)	100 300 923	95 504 262	11	95.2
Whole nodules (rbm)	134 421 425	97 500 829	13 577 676	82.6
Whole nodules (polyA)	85 897 752	82 882 874	3969	96.5
LCM fraction I	158 260 365	92 606 656	291 044	58.7
LCM fraction IId	164 272 351	84 181 779	2 755 023	52.9
LCM fraction IIp	317 819 443	92 272 619	20 974 910	35.6
LCM interzone II–III	348 611 699	95 637 275	15 080 679	31.8
LCM zone III	430 304 760	89 392 972	15 383 982	24.3
Total LCM	1 419 268 618	454 091 301	68 067 283	36.8
Pooled aerial organs	167 924 257	159 832 402	N.D.	

[a]Three biological repetitions in all cases except for pooled aerial organs (one experiment).
[b]Most of these very rare reads (<0.01% of total) correspond to rRNAs (not eliminated because not strictly included in the annotated rRNA) and are probably from traces of bacterial contamination.
Non-ambiguously mapped read pairs do not include residual tRNAs and rRNAs.
rbm, Ribominus-like; LCM, laser-capture microdissection.

(termed Mt20120830-LIPM) that combines the published Mt3.5.1 release (Young *et al.*, 2011) and assembly from whole-genome shotgun sequencing (FD, PG and JG; sequence data available on a website dedicated to our RNA-seq programme, called Symbimics: https://iant.toulouse.inra.fr/symbimics).

A summary of the RNA-seq data is given in Table 1, indicating that ≥ 940 million read pairs were unambiguously mapped, including 522 million from LCM samples. Strand specificity (determined from residual rRNA) was found to be excellent, with ≤0.01% sequences in the wrong orientation, which also indicated that contamination by genomic DNA was extremely low. Whole-organ analyses allowed us to identify 30 213 expressed *M. truncatula* mRNAs (10 or more normalized reads), among which 4354 were expressed three-fold more or greater in nodules versus roots (adjusted *P*-value < 0.01; Ribominus-like libraries), while 572 mRNAs were exclusively detected in nodules (adjusted *P*-value < 0.01). Tables S2(a) and S2(b) (supporting information and Symbimics website) provide detailed information on all detected *M. truncatula* mRNAs, including notably corresponding gene identifiers in Mt3.5.1 and Mt4.0v1 *M. truncatula* genome versions, as well as best hits found by BLAST interrogation of the TAIR and SWISSPROT protein databases. The rate of unambiguous mapping of RNA-seq reads from LCM fractions was lower than from whole organs, indicating more residual rRNA, possibly due to partial RNA degradation decreasing the efficiency of rRNA depletion. However, no severe bias was observed in the distribution of reads from LCM libraries from the 3′ to 5′ end of transcripts (see Figure S2 for an example). This contrasted with previous reports on gene expression studies following LCM, where only 3′ ends could be well detected, most likely due to a combination of partial mRNA degradation and selection of polyA+ molecules (Schmid *et al.*, 2012).

The reproducibility of the whole process was examined by scatter plot analyses (Figure S3), principal component analyses (Figure S4) and systematic pairwise comparisons of all biological repetitions (Table S1B and C). Correlation between biological repetitions was excellent for both plant and bacterial data ($R^2 > 0.95$ in most cases) and clearly better than between different fractions. These analyses also revealed that the IZ and ZIII were globally much more distinct from each other for bacterial than for plant RNAs, whereas FIId and FIIp were more different for plants than for bacteria (Figure S4).

Highly distinct plant and bacterial transcriptomes in five nodule regions

Figure 2(a) shows the number of *M. truncatula* mRNAs detected in whole organs and LCM fractions. About 34% (10 028; Table S3) and 22% (6683) of the 29 673 mRNAs detected in the LCM fractions are not represented on the current *M. truncatula* Affymetrix chip (Benedito *et al.*, 2008) and the bacterial artificial chromosome (BAC)-based Mt3.5.1 genome sequence release (Young *et al.*, 2011), respectively, showing that our study enabled a substantial enrichment in the number of genes analyzed. A comparison of the genes scored as differentially expressed between roots and mature nodules by RNA-seq (this study) and Affymetrix chip hybridization (Benedito *et al.*, 2008) indicated a good correlation ($R^2 = 0.86$).

A high proportion of *S. meliloti* genes was detected in all the LCM fractions (87%; i.e. 7799 genes, as defined in Sallet *et al.*, 2013). This contrasted with previous reports that showed only a few bacterial genes being expressed in nodules (Barnett *et al.*, 2004). We assume that this discrepancy is due to the high sensitivity of the RNA-seq approach used here. As expected, the proportion of sequencing reads of bacterial origin was very low in FI and FIId (Table 1, Figure 2b). However, some were detected in FI, suggesting some level of contamination by the rhizobium-containing ZII (estimated at about 10% by comparison with the adjacent fraction, FIId).

To validate the LCM methodology, we examined a set of marker genes previously characterized by other methods (*in situ* hybridization, reporter gene fusion, symbiosome proteomics, cDNA-amplified fragment length polymorphism and LCM-Affymetrix analysis). Table 2 shows their relative expression levels in different nodule regions (systematic pairwise comparisons of fractions are given in Tables S2b and S4 for plant and bacterial genes, respectively). Expression of meristematic markers (e.g. *MtWOX5* and *MtROP2*) was found essentially in FI, as expected. In this fraction transcripts from genes known to be expressed in the pre-infection zone (e.g. *MtERN1* and its target gene *MtENOD11*) were also detected, confirming that FI included part of the pre-infection zone. FIId contained transcripts from genes associated with pre-infection and infection processes (e.g. *MtN1*, *MtMMPL1*, *MtERN2*) as well as cell differentiation control (*MtCCS52a, MtEFD*). FIIp showed maximal expression of markers linked to proximal ZII and maturation of infected cells (e.g. *DNF1*, *MtIRE*). The IZ and ZIII showed differential accumulation of transcripts known to be associated with the symbiosome (e.g. *MtNIP1*, *MtENOD8, MtRBOHA*), indicating that these two fractions corresponded to different developmental stages.

The distribution of *S. meliloti* mRNAs was also very consistent with their known expression patterns. The *nodABC* genes, involved in the synthesis of NF, were maximally expressed in FIId, consistent with their role in (pre)-infection. The *nifA* and *fixK* genes dependent on the FixLJ two-component regulatory system, as well as genes regulated by them (e.g. *nifH* and *fixN1*) and encoding proteins involved in nitrogen fixation or micro-oxic respiration of bacteroids, were found to be maximally expressed in the IZ and ZIII. The catalase-encoding genes *katA*, *katB* and

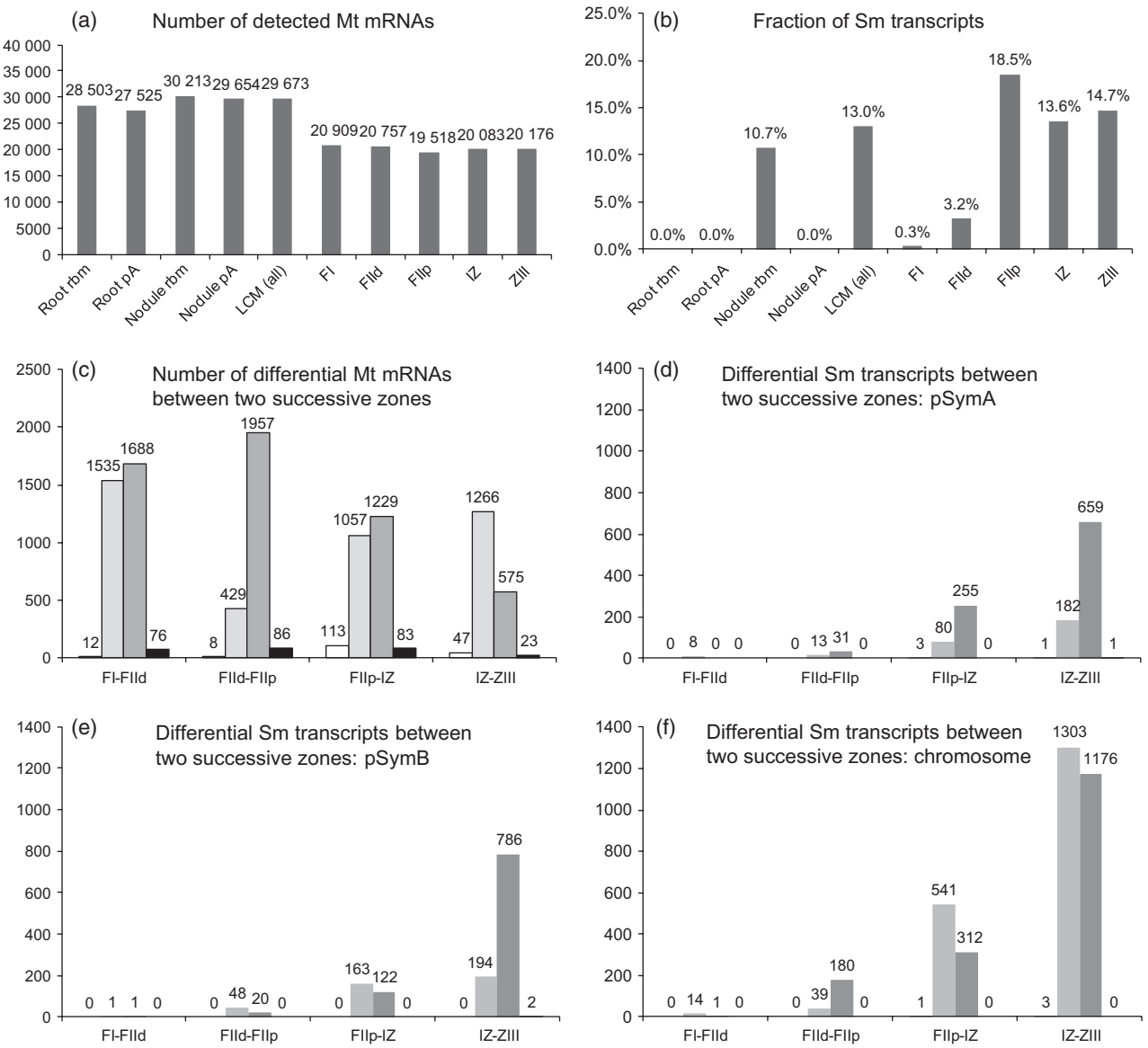

Figure 2. The RNA-seq analysis of plant and bacterial transcripts in whole organs and laser-dissected samples.
(a) Number of detected *Medicago truncatula* (Mt) mRNAs (10 or more normalized reads for three biological repetitions).
(b) Fraction of *Sinorhizobium meliloti* (Sm) transcripts versus the total number of mapped RNA-seq reads.
(c)–(f) Number of *M. truncatula* mRNAs (c) and *S. meliloti* transcripts from each replicon (d–f) showing differential expression (adjusted *P*-value < 0.01) between two successive laser-capture microdissection fractions; for each comparison the numbers of mRNAs is shown, from left to right: detected only in the most distal fraction (white bars), more highly expressed in the distal fraction (light grey), more highly expressed in the proximal fraction (dark grey), detected only in the proximal fraction (black). Rbm, Ribominus-like; pA, polyA; all, all fractions; IZ, interzone; ZIII, zone III; FI, fraction I; FIId, distal fraction II; FIIp, proximal fraction II.

katC showed zone-specific expression patterns according to previous published data: *katA* was mainly expressed in the IZ and ZIII, *katC* was preferentially expressed in FIId and ZIII, while *katB* transcripts were equally found in all LCM fractions.

Combined analysis of plant and bacterial gene expression profiles

After confirming the robustness of our LCM–RNA-seq approach, we then examined global transcriptome differences between successive nodule fractions. Strong variations of the *M. truncatula* mRNA population were detected all along the nodule. The number of mRNAs showing differential levels between two successive fractions (adjusted *P*-value < 0.01, which corresponded to a ratio of greater than two in 98.3% of the cases) ranged from 1911 (IZ–ZIII) to 3311 (FI–FIId) (Figure 2c). FIId and FIIp differed by a large number of upregulated mRNAs in the FIIp fraction, suggesting the need for new mRNAs for the differentiation process. On the contrary, more mRNAs were downregulated

Table 2 Distribution of normalized RNA-seq reads for a set of marker genes

Mt20120830-LIPM	Annotation	Published pattern	Reference	% FI	% FIId	% FIIp	% IZ	% ZIII
Medicago truncatula								
Mt0010_10219	*MtWOX5*	Nodule apex	Osipova *et al.* (2012)	97.5	2.5	0.0	0.0	0.0
Mt0001_00654	*MtN13*	Nodule apex	Gamas *et al.* (1998)	93.6	6.4	0.0	0.0	0.0
Mt0024_10233	*MtROP2*	Meristem	Limpens *et al.* (2013)	89.3	8.9	0.4	0.3	1.0
Mt0016_00146	*CYCA2;4*	Meristem	Roudier *et al.* (2003)	73.9	24.9	1.3	0.0	0.0
Mt0010_00446	*MtLYK3*	Nodule apex	Limpens *et al.* (2005)	62.0	34.5	3.3	0.0	0.2
Mt0011_10241	*MtNOOT1*	Nodule apex	Couzigou *et al.* (2012)	61.1	23.7	1.8	6.3	7.2
Mt0011_00459	*MtERN1*	ZII	Cerri *et al.* (2012)	55.8	36.1	7.9	0.1	0.0
Mt0017_10456	*MtENOD11*	ZIId	Journet *et al.* (2001)	52.1	43.0	4.9	0.0	0.0
Mt0001_00292	*MtSPK1*	Nodule apex	Andrio *et al.* (2013)	35.7	35.5	21.4	3.1	4.3
Mt0004_00583	*MtN6*	ZII	Mathis *et al.* (1999)	33.3	58.3	7.2	0.8	0.5
Mt0004_00313	*MtNF-YA1*	Nodule apex	Combier *et al.* (2006)	26.3	33.6	27.2	8.5	4.4
Mt0017_10454	*MtENOD12*	ZII	Limpens *et al.* (2013)	22.4	60.2	14.8	1.3	1.2
Mt0033_00230	*MtN1*	ZII	Gamas *et al.* (1998)	7.3	70.4	22.0	0.1	0.3
Mt0033_10028	*MtERN2*	ZII	Cerri *et al.* (2012)	9.8	65.9	10.6	13.1	0.7
Mt0012_10504	*MtRR4*	Nodule apex	Plet *et al.* (2011)	1.1	62.4	33.8	1.6	1.1
Mt0001_00212	*MtENOD20*	ZII–ZIII	Vernoud *et al.* (1999)	2.4	57.3	30.3	2.5	7.4
Mt0064_00055	*MtEFD*	ZII	Vernié *et al.* (2008)	6.2	57.0	25.9	2.6	8.2
Mt0012_10535	*MtMMPL1*	ZII	Combier *et al.* (2007)	4.9	45.9	45.1	2.5	1.5
Mt0008_00729	*MtIRE*	ZIIp	Pislariu and Dickstein (2007)	0.4	13.1	54.6	28.8	3.0
Mt0043_00134	*MtDNF1*	ZII (and ZIII)	Wang *et al.* (2010)	2.5	20.6	53.3	15.9	7.7
Mt0077_10039	*MtNAC1*	ZII and distal ZIII	D'Haeseleer *et al.* (2011)	1.1	11.2	49.9	35.3	2.5
Mt0001_11374	*MtCCS52a*	ZI–ZII	Vinardell *et al.* (2003)	4.6	25.6	47.9	12.9	9.1
Mt0001_10243	*MtENOD16*	ZII–ZIII	Catalano *et al.* (2004)	0.2	8.9	43.4	32.5	15.0
Mt0009_10577	*MtSYMREM1*	ZII–ZIII	Lefebvre *et al.* (2010)	0.7	19.4	34.2	27.3	18.4
Mt0007_10556	*MtbHLH1*	VB and ZIII	Godiard *et al.* (2011)	5.6	0.8	5.7	61.1	26.9
Mt0010_00289	*MtPUB1*	ZI–ZIII	Mbengue *et al.* (2010)	4.5	17.1	11.4	33.4	33.6
Mt0003_11544	*MtDNF2*	ZII, IZ, distal ZIII	Bourcy *et al.* (2013)	0.2	8.7	16.0	41.4	33.7
Mt0097_00015	*NCR035*	IZ–ZIII	Van de Velde *et al.* (2010)	0.0	0.9	21.6	41.7	35.7
Mt0002_00363	*MtCKX1*	ZII–ZIII	Moreau *et al.* (2011)	5.6	8.1	13.9	30.1	42.3
Mt0054_10215	*NCR001*	IZ–ZIII	Van de Velde et al. (2010)	0.0	0.1	0.7	55.8	43.3
Mt0005_01094	*MtIPD3*	ZIII	Messinese *et al.* (2007)	3.8	4.7	11.8	35.0	44.7
Mt0013_00721	*MtNOD25*	Symbiosome	Catalano *et al.* (2004)	0.0	0.1	6.5	44.8	48.5
Mt0013_00713	*MtCaML1*	IZ–ZIII	Liu *et al.* (2006)	0.0	0.1	0.4	48.4	51.1
Mt0009_00137	*MtNip1*	Symbiosome	Catalano *et al.* (2004)	0.4	0.9	7.5	22.9	68.3
Mt0002_00999	*MtENOD8.1*	ZIII	Coque *et al.* (2008)	0.1	0.1	0.2	27.0	72.6
Mt0004_00211	*MtRBOHA*	ZIII	Marino *et al.* (2011)	0.2	0.2	2.2	23.1	74.3
Mt0001_00230	*HSP70*	Symbiosome	Catalano *et al.* (2004)	1.0	0.2	0.1	0.7	98.0
Sinorhizobium meliloti								
SMa0869	*nodA*	ZI–ZII	Sharma and Signer (1990)	62.2	7.5	1.8	2.6	25.9
SMa0868	*nodB*	ZI–ZII	Sharma and Signer (1990)	42.6	16.3	4.2	4.9	32.0
SMa0866	*nodC*	ZI–ZII	Sharma and Signer (1990)	35.1	23.8	9.2	8.8	23.2
SMa1225	*fixK1*	IZ–ZIII	Soupène *et al.* (1995)	1.5	0.6	2.3	28.3	67.2
SMa0815	*nifA*	IZ–ZIII	Sharma and Signer (1990)	2.4	0.5	0.4	27.5	69.2
SMa1220	*fixN1*	IZ–ZIII	Soupène *et al.* (1995)	1.1	0.5	3.7	25.6	69.1
SMa0825	*nifH*	IZ–ZIII	Labes *et al.* (1993)	0.9	0.3	0.2	31.1	67.5
SMb20611	*dctA*	ZII–IZ–ZIII	Boesten *et al.* (1998)	4.7	14.0	4.6	44.7	32.0
SMc00819	*katA*	IZ–ZIII	Jamet *et al.* (2003)	2.1	0.9	16.5	61.4	19.1
SMb20007	*katC*	ZII and ZIV	Jamet *et al.* (2003)	0.0	20.0	8.5	8.6	63.0
SMa2379	*katB*	Non-specific	Jamet *et al.* (2003)	23.6	25.0	19.6	18.5	13.3

ZI, zone I; ZIId, distal zone II; ZIIp, proximal zone II; IZ, interzone; ZIII, zone III; VB, vascular bundles; FI, fraction I; FIId, distal fraction II; FIIp, proximal fraction II.
Identifiers beginning with Mt and SM correspond to *M. truncatula* and *S. meliloti* genes, respectively.

than upregulated in ZIII as compared to the IZ (1313 versus 598), suggesting a stronger specialization in ZIII (Figure 2c).

Only a few bacterial genes showed differential expression between FIId and FIIp. Changes in bacterial gene expression were mostly found between FIIp and the IZ and between the IZ and ZIII (1477 and 4307 differentially expressed genes, respectively), most likely related to bacteroid differentiation (Figure 2d–f). Interestingly, genes

located on each of the three bacterial replicons differentially contributed to global changes in gene expression along the nodule: whereas most (78%) upregulated genes during the FIId–FIIp transition were chromosomal, only 45% of the genes upregulated during the FIIp–IZ and IZ–ZIII transitions and most (>70%) of the repressed genes were chromosomal (Figure 2d–f).

To refine the classification of expression profiles we performed a hierarchical clustering analysis based upon the relative expression in the five LCM fractions of both plant and bacterial genes. All transcripts showing at least 50 RNA-seq reads (total of the five LCM fractions) and differential expression between at least two fractions (adjusted *P*-value < 0.01) (14 093 *M. truncatula* mRNAs and 5477 *S. meliloti* genes) were used for this analysis. Thirteen clusters could be distinguished (Figure 3). About 54% (8558) of clusterized *M. truncatula* mRNAs versus 22% (1222) of clusterized *S. meliloti* genes exhibited sharp transitions (clusters 1, 2, 3, 4, 6, 7, 9 and 10). This clustering appeared qualitatively sound, with, for example, the distinction of meristematic (cluster 1) and pre-infection (cluster 2) plant genes. The identification of differential Gene Ontology term distribution among the clusters is shown in Table S5.

We examined the spatial distribution of 2197 nodule-preferential plant mRNAs, defined as either exclusively detected in nodules or strongly upregulated (≥20-fold) in nodules 10 days post-inoculation (dpi) as compared with roots (Table S6). Very few of them were found in the nodule apex as compared with the bulk of *M. truncatula* mRNAs (Figure 4), with 3.0% versus 40.7% in clusters 1, 2, 4 and 5 respectively. Fifty-five nodule-preferential putative transcriptional regulators and 30 proteasome components, potentially impacting on specific transcript and protein accumulation, respectively, as well as 31 protein kinases, potentially regulating protein activity, were found to be expressed in different nodule zones (Tables 3 and S6, Figure 4). Most of them have never been described before and represent good candidates for the control of developmental transitions in the nodule.

A tool to access our RNA-seq data is available on the Symbimics website (https://iant.toulouse.inra.fr/symbimics). Various identifiers (from *S. meliloti* and successive *M. truncatula* genome and microarray releases) or a BLAST form can be used to query the data. Plots of absolute and/or relative RNA-seq expression data are provided, as well as transcript and protein sequences, with links to the *M. truncatula* V4 genome browser provided by the J. Craig Venter Institute (http://www.jcvi.org/cgi-bin/medicago/overview.cgi) and the *M. truncatula* gene atlas. The download section of the Symbimics site provides links to all sequence datasets and tables (with correspondence with Mt3.5.1 and Mt4.0v1 gene IDs and a grey scale for easier visualization of relative expression levels) used in this analysis.

(a)

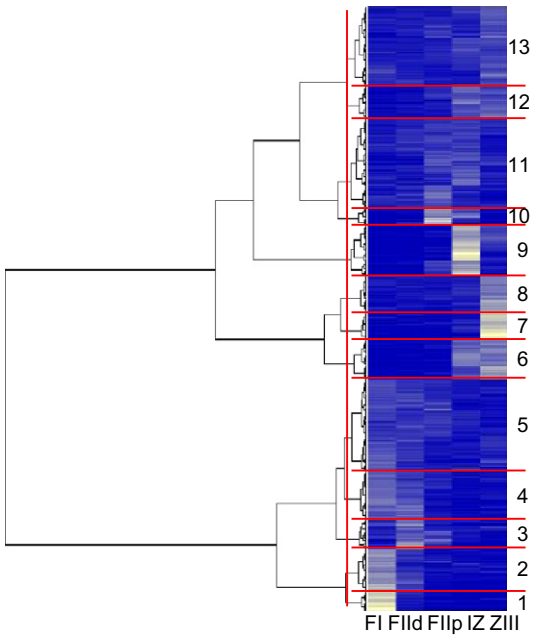

(b)

cluster	%FI	%FIId	%FIIp	%IZ	%ZIII	M.t.	S.m.
1	81	13	3	2	1	713	7
2	57	24	8	6	5	1338	83
4	41	33	13	5	7	1420	192
5	31	25	19	12	13	2269	849
3	16	48	22	7	7	735	250
11	13	17	29	28	14	1630	1336
10	1	5	61	28	4	441	18
9	1	1	10	68	20	1098	71
12	6	7	15	37	35	943	152
6	1	2	4	41	52	1039	111
7	3	3	3	12	79	427	490
8	10	11	11	15	53	353	892
13	15	15	16	21	33	1687	1026

Figure 3. Hierarchical clustering analysis of plant and bacterial RNA-seq data from laser-dissected samples.
(a) The clustering analysis with cluster numbers indicated on the right, with a blue to white color scale indicating the lowest to highest level of expression, respectively. IZ, interzone; ZIII, zone III; FI, fraction I; FIId, distal fraction II; FIIp, proximal fraction II.
(b) A summary of cluster features (mean of relative expression values in different nodule fractions for all genes of the considered cluster), including the number of plant and bacterial genes in each cluster (right two columns); clusters were ordered from maximum expression in FI (top, cluster 1) to maximum expression in ZIII (cluster 7). The two bottom clusters (clusters 8 and 13) are substantially expressed in all nodule zones. Only genes showing differential expression between at least two nodule fractions were considered.

Key regulators of the root apical meristem are expressed in the nodule meristem region

We took advantage of the sensitivity of our approach to examine gene expression associated with the nodule

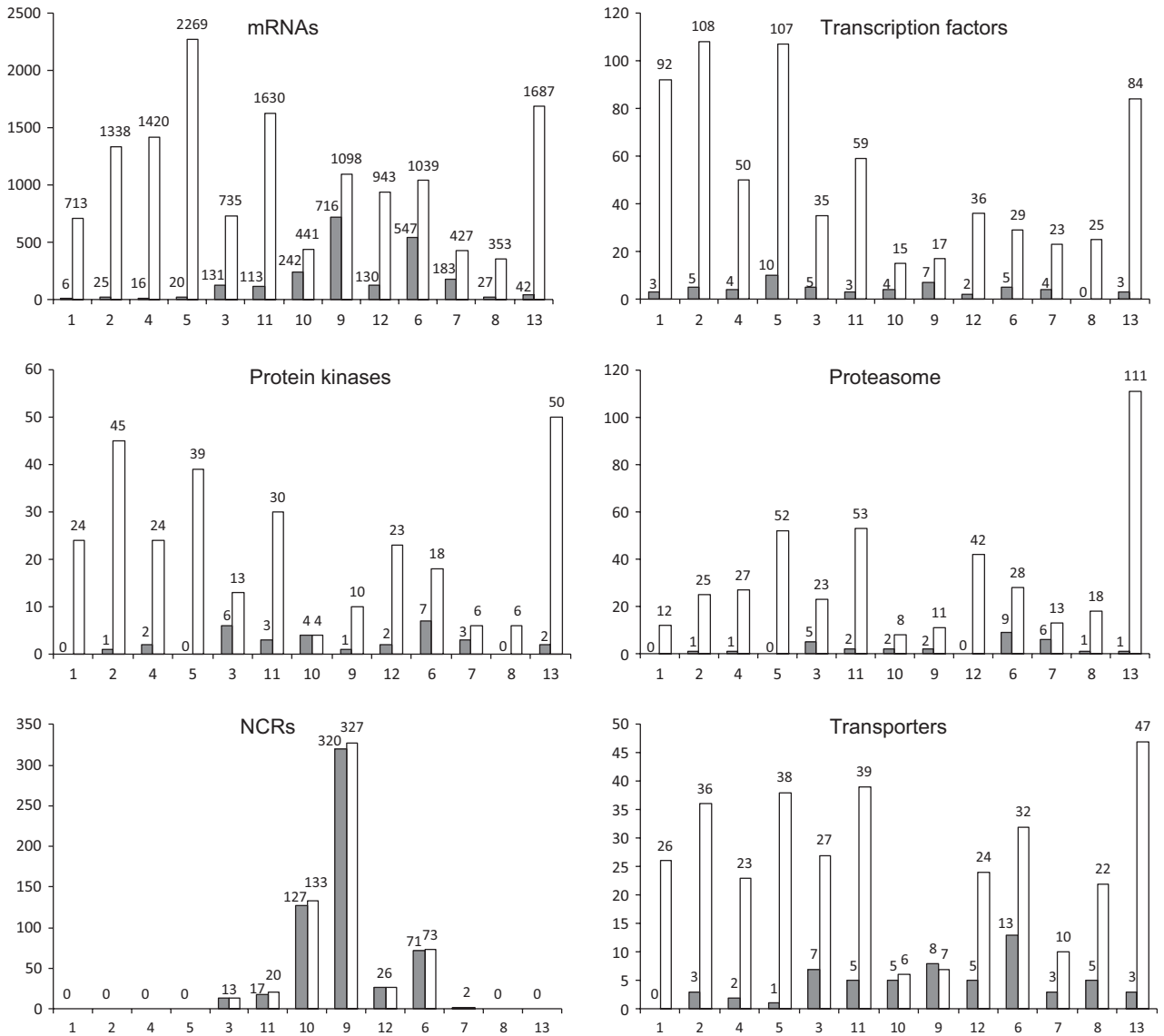

Figure 4. Distribution of highly nodule-preferential versus all expressed *Medicago truncatula* mRNAs among the 13 expression clusters.
Clusters (x axis) are ordered as in Figure 3(b), from the distal (cluster 1) to the proximal (cluster 7) nodule zones and with clusters 8 and 13 expressed in all nodule zones. Grey bars: mRNAs upregulated 20-fold or more or which are nodule-specific (adjusted *P*-value < 0.01) when comparing whole nitrogen-starved roots and 10-day-old nodules (Ribominus-like libraries). White bars: all expressed mRNAs (50 or more reads). NCRs are small cysteine-rich proteins.

meristem, which plays a crucial role in nodule formation and patterning. We addressed in particular the question of whether genes involved in the regulation of the root apical meristem (RAM) are also expressed in the nodule meristem, taking the *Arabidopsis thaliana* RAM as a model. Although *M. truncatula* roots, as in all Fabaceae, have an open RAM while *A. thaliana* has a closed RAM (Rost, 2011), it can be expected that important RAM regulators are shared between these two species.

The RAM tissues are formed from stem cells that produce cells which first divide, then elongate and finally differentiate to acquire specialized features, in the meristematic, elongation and differentiation zones, respectively (Petricka *et al.*, 2012). Stem cells surround a region of less mitotically active cells, the quiescent center (QC), which is essential for maintenance of their undifferentiated state. To date, similar domains have not been defined in the nodule apical meristem. Interestingly, close homologs for a series of key RAM regulatory genes (Petricka *et al.*, 2012) were found to be expressed in the nodule FI, belonging to cluster 1 along with cyclins A and B and cyclin-dependent kinases involved in mitosis (Table 4): WOX5, a homeodomain TF expressed in the QC; ACR4, a receptor-like kinase controlling *WOX5* expression via CLE peptide perception; PLETHORA (PLT, an AP2/ERF TF) and SHORTROOT (SHR)/SCARECROW (SCR), two GRAS TFs essential for QC speci-

Table 3 Highly preferential plant nodule genes involved in transcriptional regulation and proteasome degradation

				Ribominus-like		PolyA libraries	
Mt20120830-LIPM	Cluster	Protein Annotation	Process	Nodule	Root	Nodule	Root
Mt0003_01535	1	TF ERF	Transc. regul.	584.9	1.0	2046.6	2.8
Mt0020_00280	2	STY1	Transc. regul.	2542.8	43.6	2102.1	24.3
Mt0053_00170	2	TF ERF	Transc. regul.	1434.5	9.0	2251.9	2.9
Mt0099_10059	2	TF ERF	Transc. regul.	376.4	1.0	209.2	0.0
Mt0056_00130	2	TF ERF	Transc. regul.	1251.8	11.5	1836.7	5.7
Mt0003_01537	2	TF ERF	Transc. regul.	1033.7	2.1	1774.0	1.5
Mt0006_11009	3	MtN7 F-box protein[a]	Proteasome	4934.5	2.2	5069.5	1.6
Mt0010_10585	3	TF Zn finger	Transc. regul.	38.3	0.6	40.9	0.0
Mt0004_00313	3	MtNF-YA1[a]	Transc. regul.	5405.6	20.3	10 836.5	48.7
Mt0011_10414	3	MtN20 Zn finger, GRF type[a]	Transc. regul.	15 425.6	3.4	8931.4	5.0
Mt0010_10662	4	MtN2 ubiquitin hydrolase[a]	Proteasome	4423.7	3.2	9165.3	3.3
Mt0099_10026	5	TF ERF	Transc. regul.	2592.3	6.6	1244.2	2.2
Mt0099_10029	5	TF ERF	Transc. regul.	1547.1	10.0	948.0	0.9
Mt0099_10055	5	TF ERF	Transc. regul.	473.1	2.3	317.6	0.9
Mt0056_00132	5	TF ERF	Transc. regul.	2030.9	15.3	1165.3	2.7
Mt0056_00133	5	TF ERF	Transc. regul.	871.5	8.1	441.2	0.7
Mt0006_11056	6	F-box protein	Proteasome	897.2	0.0	1286.5	0.0
Mt0002_10286	6	TF WRKY	Transc. regul.	4634.2	36.9	1532.5	17.4
Mt0013_10514	6	E3 ligase[a]	Proteasome	11 269.4	8.6	7333.3	6.3
Mt0006_11070	6	F-box protein	Proteasome	374.0	1.2	231.7	0.7
Mt0047_10201	6	F-box protein	Proteasome	12 488.0	25.5	24 800.0	19.4
Mt0017_00232	6	F-box protein	Proteasome	495.3	0.0	66.0	0.0
Mt0097_10015	6	SKP1-like	Proteasome	173.3	0.0	175.8	1.8
Mt0003_00553	6	TF WOX	Transc. regul.	297.4	1.8	401.8	0.0
Mt0046_00224	7	E3 ligase	Proteasome	31 818.8	33.8	29 153.8	19.1
Mt0006_11071	7	F-box protein	Proteasome	1681.3	0.0	1805.6	0.7
Mt0001_00787	7	F-box protein	Proteasome	10 377.1	18.7	6073.7	15.7
Mt0002_01502	7	TF ERF	Transc. regul.	827.3	0.4	864.2	3.8
Mt0061_10029	7	TF Zn finger	Transc. regul.	41.3	0.0	25.7	0.0
Mt0086_10022	9	TF ZnFg C2H2[a]	Transc. regul.	13 104.8	3.4	8404.1	2.5
Mt0008_01043	9	TF Zn finger	Transc. regul.	485.9	6.8	2852.8	19.2
Mt0048_10243	9	F-box protein	Proteasome	1009.6	1.6	710.1	0.0
Mt0015_00073	9	TF ERF	Transc. regul.	305.6	2.1	428.0	1.6
Mt0008_10358	9	F-box protein[a]	Proteasome	5254.0	6.0	3982.0	0.0
Mt0004_10707	9	Zn finger, GRF type[a]	Transc. regul.	29 331.4	8.0	31 424.8	18.1
Mt0002_00197	10	F-box protein	Proteasome	57.5	0.6	81.3	0.0
Mt0021_00272	10	TF MYB	Transc. regul.	970.7	1.5	462.3	1.5
Mt0010_01109	11	TF MtNIN[a]	Transc. regul.	35 519.1	206.9	33 108.4	193.0
Mt0099_10028	13	TF ERF	Transc. regul.	3855.2	70.6	2413.8	10.3
Mt0056_00131	13	TF ERF	Transc. regul.	2254.0	24.7	1131.8	9.2
Mt0008_00566	13	E3 ligase	Proteasome	16 466.7	7.7	16 895.4	20.1

[a]Indicates a gene only found expressed in nodules, based on the *Medicago truncatula* gene atlas data (as of July 2013). The four right columns indicate normalized RNA-seq values from whole-organ libraries (means of three repetitions).
TF, transcription factor.

fication and RAM cell division; JACKDAW (JKD), a C2H2 zinc finger TF necessary for SCR expression; FEZ and SMB, two NAC domain TFs that control RAM initials involved in the lateral root cap and columella production. Transcripts of *M. truncatula* orthologs of *AtBABYBOOM1* (*BBM1*), that encodes an ERF proposed to promote cell proliferation and morphogenesis (Boutilier *et al.*, 2002) and *LATERAL ORGAN BOUNDARY* (*AtLBD16*), that codes for a regulator of lateral root formation (Okushima *et al.*, 2007) were also detected in cluster 1 (Table 4).

In the RAM, cell expansion following cell division is associated with specific expression of the tonoplast aquaporin GAMMA-TIP that enables vacuole expansion and is regulated by the GPI-anchored protein COBRA (Petricka *et al.*, 2012). Very consistently, the *M. truncatula* orthologs of the two corresponding genes were found to be maximally expressed in FIId and to a lesser extent in FI (Tables 4 and S2).

In the RAM and the nodule apical meristem, differentiation is strongly correlated with the onset of endocycles

Table 4 Candidate genes involved in the control of the nodule meristem and differentiation

Mt20120830-LIPM	Cluster	Annotation	Total reads LCM	Nodule/root ratio[a]	% FI	% FIId	% FIIp	% IZ	% ZIII
Medicago truncatula									
Mt0016_10327	1	*ACR4 CRINKLY4*	360.2	0.47	88.3	4.9	4.4	1.2	1.1
Mt0011_00702	1	*BABY BOOM1*	1587.7	2.11	94.3	5.5	0.2	0.0	0.0
Mt0004_01108	1	*CDKB2;2*	3064.0	0.17	77.2	20.2	2.5	0.1	0.0
Mt0006_10070	1	*CYCA1;1*	631.9	0.10	78.2	17.0	4.2	0.5	0.0
Mt0104_00013	1	*CYCB3;1*	594.5	0.25	76.6	21.2	0.7	0.0	1.4
Mt0012_10340	1	*FEZ*	100.1	0.31	93.1	6.9	0.0	0.0	0.0
Mt0004_10725	1	*JKD JACKDAW*	514.2	1.93	82.9	10.2	3.1	3.7	0.2
Mt0043_10032	1	*LBD16*	305.0	0.21	94.5	5.3	0.0	0.0	0.2
Mt0006_00996	1	*MtCCS52b*	410.0	0.32	79.8	18.3	2.0	0.0	0.0
Mt0011_10263	1	*MtPIN10*	657.7	0.50	93.1	4.5	2.4	0.0	0.0
Mt0082_00042	1	*MtPIN4*	147.7	0.14	87.5	11.5	0.0	0.0	1.1
Mt0010_10219	1	*MtWOX5*	196.4	3.36	97.5	2.5	0.0	0.0	0.0
Mt0016_00349	1	*PLT2*	417.2	0.70	98.4	1.4	0.0	0.2	0.0
Mt0026_10342	1	*SCR SCARECROW*	1027.3	1.06	84.5	12.1	1.3	2.0	0.2
Mt0005_10514	1	*SHR SHORTROOT*	87.2	0.31	88.6	10.9	0.5	0.0	0.0
Mt0004_01131	1	*SHY2*	872.3	0.50	94.8	4.8	0.3	0.0	0.1
Mt0064_10015	2	*CDKB1;2*	1271.8	0.15	52.5	29.7	17.2	0.1	0.5
Mt0016_00146	2	*CYCA2;4*	387.3	0.24	73.9	24.9	1.3	0.0	0.0
Mt0004_00313	3	*MtNF-YA1*	33 950.1	265.75	26.3	33.6	27.2	8.5	4.4
Mt0072_10022	3	*COBRA*	667.9	0.08	26.0	61.9	8.7	2.1	1.3
Mt0009_10996	5	*MtCRE1 = HK4*	4658.7	0.71	30.4	13.6	11.7	27.6	16.7
Mt0002_10081	3	*YUCCA*	136.9	0.15	16.4	37.8	42.6	3.1	0.0
Mt0013_00342	4	*CDC6*	466.1	0.07	38.7	48.5	12.4	0.4	0.0
Mt0027_00383	4	*HIGH PLOIDY2*	584.7	0.54	42.8	28.4	13.9	4.9	9.9
Mt0001_00606	4	*MCM2*	2259.8	0.16	44.1	40.6	14.9	0.1	0.3
Mt0001_11722	4	*MCM3*	2865.7	0.49	51.9	33.9	13.8	0.3	0.0
Mt0003_10882	4	*MCM4*	1878.5	0.25	42.0	34.3	22.6	0.6	0.6
Mt0001_10832	4	*MCM5*	2209.8	0.25	50.5	36.1	13.3	0.1	0.1
Mt0009_10280	4	*MCM6*	2786.7	0.23	51.8	35.9	12.2	0.1	0.1
Mt0002_10509	4	*ORC2*	227.6	0.12	46.5	45.4	8.1	0.0	0.0
Mt0012_10352	4	*ORC6*	1004.7	0.28	39.4	39.2	20.1	0.2	1.0
Mt0001_11374	11	*MtCCS52a*	8226.2	0.84	4.6	25.6	47.9	12.9	9.1
Mt0064_00055	3	*MtEFD*	6584.8	8.64	6.2	57.0	25.9	2.6	8.2
Mt0012_10504	3	*MtRR4*	5349.5	6.64	1.1	62.4	33.8	1.6	1.1
Mt0006_00055	3	*ARR19*	16 863.3	4.55	12.0	55.5	30.8	1.5	0.1
Mt0002_00363	12	*MtCKX1*	2458.9	5.19	5.6	8.1	13.9	30.1	42.3
Mt0055_10053	3	*CKX*	3110.6	0.17	23.6	58.6	17.0	0.5	0.3
Mt0012_00668	13	*TAA1-like*	197.3	22.84	1.2	28.1	36.4	4.2	30.1
Mt0031_10069	13	*YUCCA*	160.8	4.18	9.2	7.7	27.9	18.6	36.7
Mt0003_00987	9	*KRP3*	2478.7	4.01	2.8	2.4	9.3	52.0	33.5
Sinorhizobium meliloti									
SMc03808	4	*ftsK*	2678.4	n.a.	40.7	31.7	12.9	4.1	10.5
SMb20595	4	*ftsK2*	2599.2	n.a.	42.4	24.9	12.4	1.8	18.5
SMc01872	4	*ftsQ*	2436.6	n.a.	34.0	37.0	22.7	2.3	4.0
SMc01873	5	*ftsA*	3190.0	n.a.	33.1	35.4	24.3	2.9	4.2
SMc01874	4	*ftsZ1*	4495.1	n.a.	31.2	36.6	21.9	4.1	6.2
SMc04296	5	*ftsZ2*	4760.3	n.a.	31.1	29.2	17.0	5.4	17.3
SMb21522	4	*minE*	2032.6	n.a.	38.5	33.3	16.0	2.9	9.3
SMb21523	4	*minD*	2834.4	n.a.	42.5	34.2	9.5	1.9	11.8
SMb21524	4	*minC*	4708.1	n.a.	46.3	27.5	16.8	1.5	7.9
SMc01167	11	*dnaA*	53 091.9	n.a.	13.7	22.1	33.3	23.2	7.8
SMb20044	13	*repC1*	3239.0	n.a.	12.6	17.5	31.4	9.8	28.6
SMa2391	13	*repC2*	3218.3	n.a.	17.5	15.7	33.0	7.3	26.5
SMc00776	5	*cbrA*	6153.1	n.a.	25.3	20.2	29.6	17.1	7.9
SMc00021	4	*ccrM*	1164.9	n.a.	36.3	38.1	18.3	3.9	3.3
SMc00654	4	*ctrA*	24 452.4	n.a.	36.5	35.2	12.5	11.5	4.2

(continued)

Table 4. (continued)

Mt20120830-LIPM	Cluster	Annotation	Total reads LCM	Nodule/root ratio[a]	% FI	% FIId	% FIIp	% IZ	% ZIII
SMc00059	4	*divJ*	2316.5	n.a.	46.4	33.8	14.5	3.0	2.2
SMc01371	4	*divK*	1250.5	n.a.	36.5	37.5	16.1	5.2	4.6
SMc00471	5	*cckA*	3889.0	n.a.	27.5	26.7	23.9	13.2	8.7
SMc04011	2	*tacA*	1102.9	n.a.	65.5	16.5	8.7	4.2	5.0

[a]Nodule/root ratios were determined from whole-organ RNA-seq data.
All values are means from three biological repetitions.
Corresponding Affymetrix identifiers are indicated when available in Table S2. Identifiers beginning with Mt and SM correspond to *M. truncatula* and *S. meliloti* genes respectively.
RR, response regulator; LCM, laser-capture microdissection; IZ, interzone; ZIII, zone III; FI, fraction I; FIId, distal fraction II; FIIp, proximal fraction II; n.a., not applicable.

(Kondorosi and Kondorosi, 2004; Vanstraelen *et al.*, 2009). In nodules this switch involves CCS52A, a protein of the anaphase-promoting complex/cyclosome (APC/C) that controls the destruction of A- and B-type cyclins and other mitotic regulators. As expected, *CCS52A* expression was not detected in FI, in contrast to *CCS52B*, a *CCS52A* homolog involved in M-phase progression (Tarayre *et al.*, 2004), and *HIGH PLOIDY2*, a repressor of endocycle onset.

Phytohormones play a critical role in regulating cell divisions and differentiation in the RAM. Auxins positively control cell proliferation, via PLT2, whereas CKs act antagonistically to promote cell differentiation, notably via activating expression of *SHORT HYPOCOTYL2* (*SHY2*)/*IAA3*, that inhibits the auxin pathway and *PIN* expression. In the nodule various expression profiles were observed for different gene family members related to auxin and CKs (Table S7), suggesting a complex situation. Nevertheless, we found that several genes probably involved in auxin biosynthesis (Mano and Nemoto, 2012), such as a nodule-induced *TAA1*-like gene, were mostly detected in FII. The RNA-seq data also indicated that both auxin efflux *PIN* and influx *LAX* genes were particularly expressed in nodule FI (cluster 1; Tables 4 and S7), suggesting a flux of auxin toward the nodule apex. In contrast to the RAM situation, we also found that a CK-induced *SHY2*/*IAA3*-like gene (Ariel *et al.*, 2012) and a *PLT2*-like gene seemed to be expressed in the same nodule region (cluster 1, Table 4). *MtCRE1*, the most highly expressed CK receptor gene in nodules, and several TF genes predicted to positively control CK-activated genes (type B response regulators and cytokinin response factors; Hwang *et al.*, 2012) were notable in clusters 2 and 5, i.e. maximally expressed in FI and FIId (Tables 4 and S7). This is consistent with CK activity in the nodule apex, in agreement with previous data (Lohar *et al.*, 2006; Plet *et al.*, 2011). The RNA-seq data also indicated, extending previous observations (Vernié *et al.*, 2008; Moreau *et al.*, 2011; Plet *et al.*, 2011), that several negative regulators of the CK pathway (notably the type A response regulators MtRR4 and ARR19 and two CK oxidases) are strongly expressed from the start of the differentiation zone (cluster 3), like *MtEFD,* which activates the transcription of *MtRR4*.

To validate these results and obtain more precise spatial information, we performed *in situ* mRNA hybridizations using the QuantiGene ViewRNA assay (Affymetrix) (Figure 5). We used probe sets to *M. truncatula* genes orthologs of Arabidopsis genes associated with the QC (*WOX5*, *SCR*), cell division (*PLT2*) or differentiation (*SHY2*) in the RAM. In addition *MtEFD,* which was previously shown to be expressed in ZII by promoter:GUS fusion and a different *in situ* hybridization technique (Vernié *et al.*, 2008), was used as an internal control. Hybridization signals indicated that all tested genes were expressed at the tip of nodule vascular bundles. A similar expression pattern was observed for *SHY2*, *PLT2* and *SCR*, while *WOX5* showed a more localized expression pattern in the meristematic region and *MtEFD* transcripts were restricted to the distal ZII, consistent with RNA-seq data.

These results thus indicate that a number of genes known to control cell division and root patterning are expressed in the nodule apex, but possibly with a different regulation. The very localized expression profile of *WOX5* transcripts in the nodule ZI is intriguing. Whether this reflects the existence of a QC-like center in the nodule meristem is an open question which will require further study.

Gene expression associated with differentiation processes

Most of the genes strongly upregulated in nodules as compared with roots were found expressed outside the meristematic region (Figure 4), showing that the acquisition of features particular to nodules is intimately connected to the differentiation process and plant–bacteria interactions, some aspects of which are briefly presented below.

Expression of endoreduplication-related genes stops at the interzone II–III. As already mentioned, plant cell endoreduplication is positively controlled by *CCS52A,* found here to be expressed in FIId and maximal in FIIp (Table 2). A set

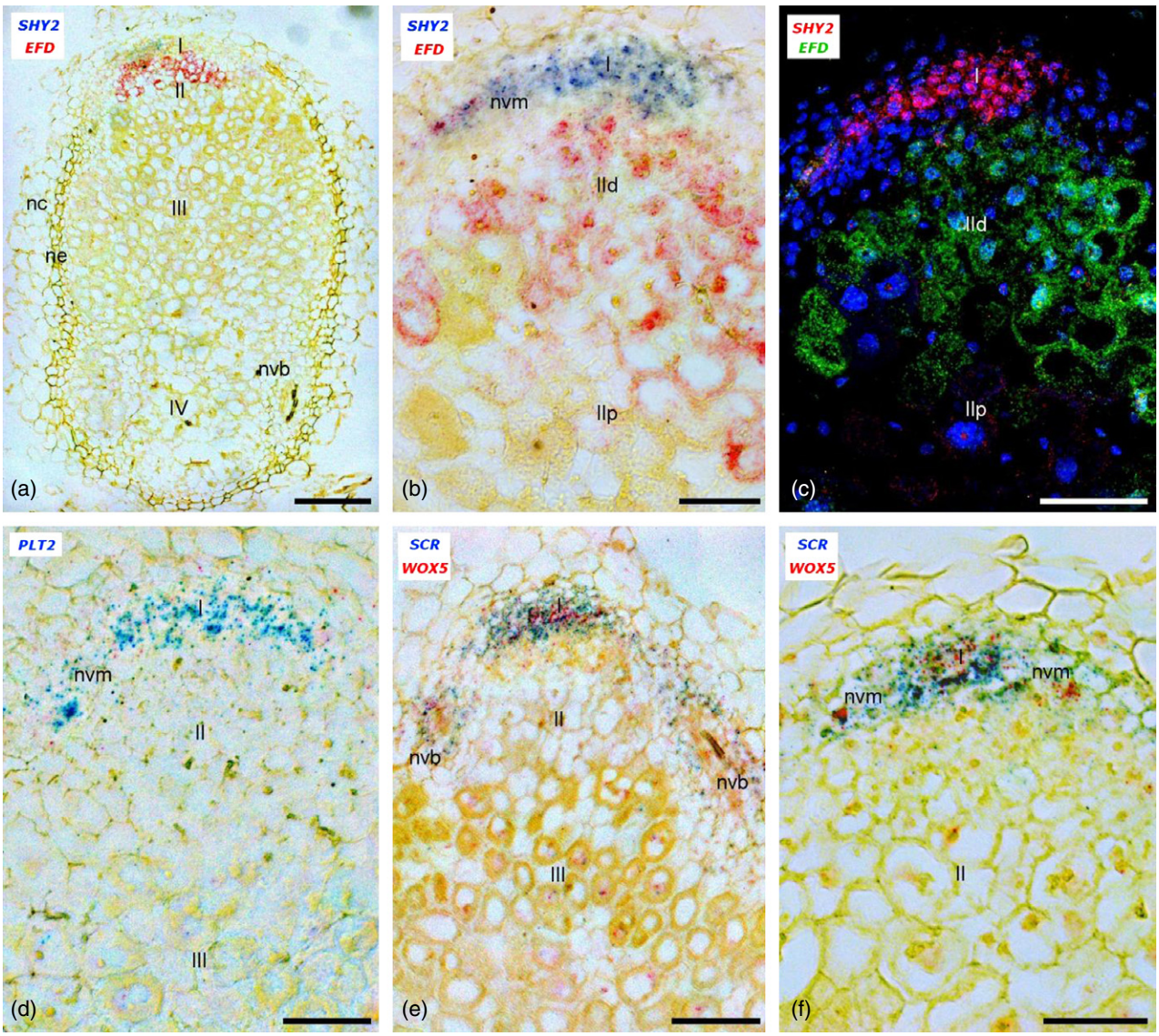

Figure 5. Gene expression analysis within the apical zone of *Medicago truncatula* nodules by *in situ* hybridization.
Hybridization signals are identified as red or blue in bright field images or as a fluorescent signal. Probes were designed from *M. truncatula* genes. (a), (b) *SHY2* (blue; best BLASTP hit against *Arabidopsis thaliana* proteins = NP_171920.1, 62% identity), *MtEFD* (red). (c) Overlay of the fluorescent signal from *SHY2* (red), *MtEFD* (green) and 4′,6-diamidino-2-phenylindole to visualize nuclei (blue). (d) *PLT2* (best *A. thaliana* hit = NP_175530.2, 83% identity). (e), (f) *SCR* (blue; best *A. thaliana* hit = NP_190990.1, 59% identity), *WOX5* (red; best *A. thaliana* hit = NP_187735.2, 61% identity). *MtEFD* is expressed in zone II. *SHY2*, *PLT2*, *SCR* and *WOX5* are expressed in the central meristematic region and the vascular meristems (in which *SCR* and *WOX5* are expressed in the vascular endodermis and the central tissue respectively). I, II, III and IV are nodule zones I, II (d, distal; p, proximal), III and IV. Nc, ne, nvb, nvm are nodule cortex, endodermis, vascular bundle, vascular meristem. Scale bars: (a) 200 μm; (b), (d), (f) 50 μm; (c), (e) 100 μm.

of genes required for DNA replication, namely *CDC6*, *ORC2, ORC6* and *MCM2-6* were found to be well expressed from FI to FIIp (cluster 4; Tables 4 and S5), consistently with their likely implication in mitosis and endoreduplication (Kondorosi and Kondorosi, 2004). The mitosis-specific gene *CYCA2* was mostly expressed in FI, while inhibitors of cyclin-dependent kinases (known as ICK or KRP), which are detrimental to endoreduplication, were preferentially expressed in the IZ and ZIII (Table 4). This strongly suggests that the endoreduplication process stops at the IZ. Similarly, most of the bacterial genes involved in division (*ftsQAZ*, *ftsK*, *minCDE*), initiation of DNA replication (*dnaA, repC1, repC2*) and cell cycle control (*ctrA*, *cbrA*, *tacA*, *ccrM, divJ,* . . .) were maximally expressed in FIId and FIIp, with a strong decrease in the IZ or ZIII (clusters 2, 4, 5; Table 4). This suggests coordination of plant and bacterial endoreduplication processes.

Plant cell differentiation: NCR and transporter gene expression. Genes preferentially expressed in nodules included

61 nodulin genes previously identified, as well as 576 putative NCR genes. Those were found to be activated in four waves (Figure 4), with a few of them expressed early and transiently after bacterial release (cluster 3) while others were activated respectively in FIIp (cluster 10), the IZ (clusters 9, 6; peak of activation with 411 genes) and ZIII (cluster 7). The four subunits of the signal peptidase complex involved in NCR maturation (Wang *et al.*, 2010) showed similar expression profiles, with *DNF1*, *DAS12* and *DAS25* genes in cluster 11 and *DAS18* in cluster 10 (i.e. maximal expression in FIIp and the IZ). The *S. meliloti bacA* gene was in cluster 11 as well, consistent with the described BacA function in protection of the bacterium against the cytotoxic effects of NCR peptides (Haag *et al.*, 2011).

Plant transporter genes preferentially expressed in nodules were essentially expressed in the differentiation and nitrogen-fixation zones (Figure 4, Table S6) in striking contrast to the distribution of all plant transporter genes (Figure 4). They are likely to play a key role in metabolic exchanges between the plant and bacteria or between plant cells (Udvardi and Poole 2013). Good examples are the *M. truncatula* ortholog of the *LjSST1* sulfate transporter gene (Krusell *et al.*, 2005), a molybdate transporter and peptide transporters, possibly involved in dicarboxylic acid transport as described in *Alnus glutinosa* nodules (Jeong *et al.*, 2004).

Bacteroid differentiation: expected and unexpected gene expression patterns. Ultrastructural and genetic studies have demonstrated that bacterial differentiation occurs from ZIId to the IZ, to give rise to terminally differentiated bacteroids in ZIII that, as organelle-like structures, are specialized in the fixation of atmospheric nitrogen. Consistent with the transition to a less active mature bacteroid state, most bacterial genes encoding components of the transcriptional (core RNA polymerase subunits) and translational (ribosomal proteins) machineries were strongly downregulated in the IZ or ZIII. In a similar way, the expression of the housekeeping gene encoding the sigma factor RpoD declined while the expression of the *rpoN* gene gradually increased from FIId to ZIII. Consistently, the expression of *dctBD*, involved in the transport of dicarboxylic acids (a major carbon source) and NifA-dependent genes, controlling nitrogenase complex formation, was found upregulated in the IZ and is dependent on RpoN.

Transporter genes (mainly of carbon substrates) represented more than a third of the 90 bacterial genes belonging to clusters 1 and 2. They were downregulated in FII versus FI, indicating a specialization of transport when bacteria start differentiating. Specific bacteroid requirements were suggested by the pattern of transporters from other clusters. For instance molybdenum transporters (*modAB*) were maximally expressed in the IZ and ZIII (cluster 12), consistent with the requirement of molybdenum for nitrogenase activity.

An unexpected observation was the expression in ZIII of bacterial genes involved in chemotaxis, motility and plasmid conjugation, which was validated by transcriptional *lacZ* fusion analysis for two of them (*visN* and SMc03023; Figure 6). *visN* encodes a master regulator of the flagellar regulon (Sourjik *et al.* 2000) and its upregulation in ZIII may explain the activation of the whole regulon. The biological significance of this activation, if any, is currently unknown.

Although flagellar genes were expressed in all bacteroid-containing cells of ZIII, we cannot rule out that some genes are not expressed in nitrogen-fixing bacteroids but rather in bacteria contained within ITs, or bacteria entering a saprophytic lifestyle within few cells of ZIII presenting early senescence. This seems to be the case for the *nodA* and *nodJ* genes (Figure 6, and see below). Although no visual sign of senescence was detected in laser-dissected nodules, a strong *lacZ* expression was observed in some ZIII cells of nodules induced by a bacterial strain constitutively expressing *lacZ* (*hemA:lacZ,* Figure 6), reminiscent of cells in the saprophytic zone described by Timmers *et al.* (2000). In addition, RNA-seq data revealed activation of some plant senescence marker genes in ZIII (cysteine proteinase genes, MtNAC969 TF; Van de Velde *et al.*, 2006; de Zelicourt *et al.*, 2012). Finally, many bacterial genes specifically controlled by the NO-responsive regulator NnrR (Meilhoc *et al.*, 2010) were upregulated in ZIII, suggesting a local increase in the NO level, recently proposed to trigger nodule senescence (Cam *et al.*, 2012).

Other genes were unexpectedly found downregulated in ZIII, such as those encoding the enzymes of the tricarboxylic acid (TCA) cycle, needed for assimilation of dicarboxylic acids. A possible explanation is that these transcripts or proteins are stable enough to allow the TCA cycle to work efficiently throughout ZIII. Nevertheless, Vasse *et al.* (1990) described that ZIII of alfalfa nodules could be subdivided in a distal nitrogen-fixing part and a more proximal part in which bacteroids cease nitrogen fixation. The downregulation of the TCA genes in ZIII may explain why bacteroids rapidly stop nitrogen fixation.

Gene expression associated with plant–bacteria signaling processes

Numerous signaling processes are likely to take place in the nodule, including those related to Nod factors, oxygen and reactive oxygen species.

Nod factor signaling in the pre-infection and nitrogen-fixation zones. Several genes participating in the early NF signaling pathway in the root are expressed in the pre-infection zone, raising the question of whether signaling responses in this region mimic early NF signaling

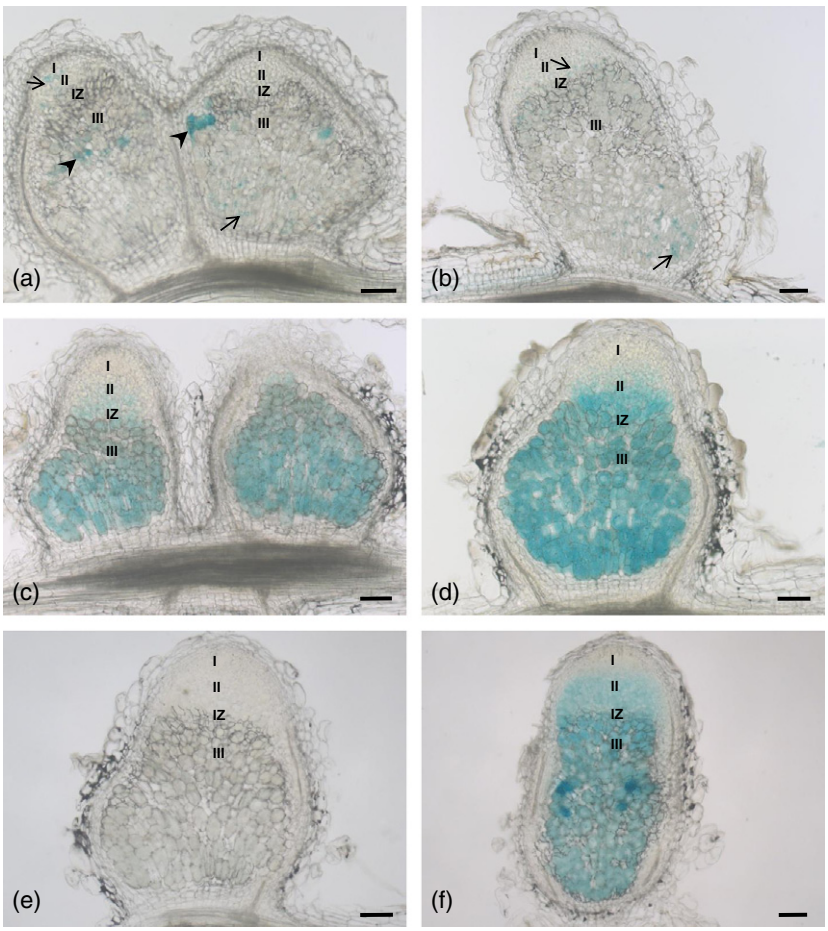

Figure 6. Expression pattern of *lacZ* transcriptional fusions for *Sinorhizobium meliloti* genes in 14-day-old nodules.
Gene expression is visualized by β-galactosidase activity (blue color): (a) *nodA* (70 min of staining); (b) *nodJ* (190 min of staining); (c) SMc03023 (40 min of staining); (d) *visN* (20 min of staining); (e) empty pCZ962 vector control (40 min of staining); (f) *hemA* (7 min of staining). *nodA* and *nodJ* expression is observed within infection threads (arrows) in nodule zones II and III, as well as occasionally in a few individual invaded cells within zone III (arrow heads). SMc03023 and *visN* show a strong increase of expression in all infected cells of zone III. *hemA* constitutive expression marks the presence of bacteria in zones II and III. I, II, III, nodule zones I, II, III; IZ, interzone II–III. Scale bars: 100 μm.

responses that occur in roots. In support of this hypothesis, 82% of the genes induced two-fold or more in roots by purified NF (Czaja *et al.*, 2012) were expressed in LCM nodule samples, in particular in FI and FIId (63.4% of clusterized transcripts in clusters 1–4) (Table S2a).

A first group of NF signaling-related genes were mostly expressed in the distal part of the nodule (*MtLYK3*, *MtNFP, MtNSP2*, *MtERN1,* ...; Table 5) whereas a second group (*DMI1*, *DMI2*, *DMI3*, *IPD3,*...) showed similar or even stronger expression in the IZ and ZIII. This is consistent with *M. truncatula* gene atlas data showing higher expression of group 2 genes in mature than in young nodules, and suggests that NF signaling is active in ZIII. This might involve MtLYR2 and/or MtLYR4, two LysM receptors expressed in ZIII (Table 5). The expression of *MtNFP* and *MtLYK3* was by contrast restricted to FI/FII suggesting a specialization of these receptors during early stages of NF signaling and infection. Supporting the existence of NF signaling in ZIII, bacterial NF biosynthesis genes (*nodABC* operon, *nodEF*, *nodH*, *nodL*) were not only expressed in FIId but also in ZIII (Table 5). Figure 6 shows that expression of *nodA* and *nodJ lacZ* transcriptional fusions was in most cases found in ITs, but in addition, as mentioned above, a few infected cells exhibited a strong *lacZ* expression. This contrasts with previous findings in *Rhizobium leguminosarum*-induced nodules of vetch or pea, in which *nod* gene expression was not detected in ZIII (Schlaman *et al.*, 1991; Marie *et al.*, 1994; Karunakaran *et al.*, 2009). Our RNA-seq results, however, are consistent with data obtained in 17-day-old alfalfa nodules showing the expression in ZIII of a *nodC*::GUS fusion (Sharma and Signer, 1990). It is thus conceivable that NF production and signal transduction take place not only in the nodule infection zone but also in ZIII, where it might be associated in particular with ITs.

Oxygen and reactive oxygen species in the control of plant and bacterial genes. The concentration of free oxygen in the nodule, which decreases from ZI to ZIII, is an important element for the regulation of some bacterial and plant genes in nodules. As expected, we found a series of leghemoglobin genes, essential for maintaining micro-oxic conditions for nitrogenase and energy production (Ott *et al.*, 2005), that were massively upregulated at the IZ (Table S2). It has been proposed that micro-oxic conditions activate the expression of the respiratory burst oxidase homolog *MtRBOHA* gene, producing reactive oxygen species

Table 5 Nodule-associated signaling-related genes

Mt20120830-LIPM	Annotation	Total reads LCM	Nodule/root ratio[a]	% FI	% FIId	% FIIp	% IZ	% ZIII
Medicago truncatula								
Mt0010_00446	*MtLYK3*	481.3	0.3	62.0	34.5	3.3	0.0	0.2
Mt0005_00682	*MtNFP*	738.3	0.2	69.9	28.6	1.0	0.5	0.1
Mt0006_00755	*MtNSP2*	1601.4	0.4	57.5	31.7	9.9	0.7	0.1
Mt0011_00459	*MtERN1*	4218.4	0.9	55.8	36.1	7.9	0.1	0.0
Mt0017_10456	*MtENOD11*	8764.5	449.4	52.1	43.0	4.9	0.0	0.0
Mt0004_00313	*MtNF-YA1*	33 950.1	265.7	26.3	33.6	27.2	8.5	4.4
Mt0005_01074	*MtHMGR1*	47.1	3.9	77.6	17.3	0.8	0.0	4.3
Mt0042_10115	LjNENA-like	584.6	0.9	38.4	25.9	11.0	10.1	14.5
Mt0010_01035	NUP133-like	1022.4	0.7	43.7	29.4	12.5	4.2	10.1
Mt0002_10011	NUP85-like	1357.0	1.0	46.0	31.1	14.9	1.9	6.0
Mt0028_00160	*MtNSP1*	1597.8	2.4	44.0	22.8	8.5	13.5	11.2
Mt0023_10495	*MtDMI1*	3140.4	2.4	5.8	4.8	2.1	22.2	65.0
Mt0012_10766	*MtDMI2*	7033.2	1.6	22.5	11.2	5.8	22.6	37.8
Mt0010_00289	*MtPUB1*	2662.3	1.8	4.5	17.1	11.4	33.4	33.6
Mt0041_00009	*MtDMI3*	13 040.3	1.4	22.4	17.9	13.2	22.3	24.2
Mt0009_10577	*MtSYMREM1*	26 443.9	4226.6	0.7	19.4	34.2	27.3	18.4
Mt0005_01094	*MtIPD3*	14 778.2	4.9	3.8	4.7	11.8	35.0	44.7
Mt0011_10464	Apyrase-like	1417.9	0.72	6.5	20.2	15.8	35.5	22.1
Mt0002_10566	*MtLYR2*	365.0	1.45	7.4	50.2	14.2	11.2	17.1
Mt0010_00422	*MtLYR4*	348.0	3.63	28.7	8.7	8.1	20.1	34.4
Mt0006_10523	*MtN23* AO	9701.3	1.8	43.8	23.9	15.1	11.4	5.8
Mt0005_00683	RLK	1775.4	798.3	17.0	50.3	27.4	4.8	0.6
Mt0014_00127	Ser/Thr protein kinase	2702.9	162.4	0.3	16.1	54.2	28.6	0.8
Mt0125_00034	LRR RLK	14 019.5	993.3	0.0	3.3	48.7	45.6	2.4
Mt0009_00747	Phospholipase A2	5427.1	1533.4	0.1	1.0	25.7	63.8	9.5
Mt0006_00443	CR RLK	22 076.7	481.8	0.8	5.3	8.9	36.2	48.7
Mt0048_00096	LRR RLK	421.4	209.1	0.1	0.7	0.0	48.4	50.8
Mt0003_00278	Ser/Thr protein kinase	36 263.7	1689.2	0.0	0.1	5.6	49.6	44.7
Mt0036_10150	Calcium/lipid-binding	1144.0	95.0	0.4	1.1	7.9	35.2	55.3
Sinorhizobium meliloti								
SMa0863	*nodJ*	666.3	n.a.	32.91	20.9	6.0	15.3	24.8
SMa0866	*nodC*	1137.2	n.a.	37.2	22.6	9.3	8.6	22.3
SMa0868	*nodB*	381.5	n.a.	42.6	16.3	4.2	4.9	32.0
SMa0869	*nodA*	575.1	n.a.	62.2	7.5	1.8	2.6	25.9
SMa0851	*nodH*	8130.7	n.a.	12.8	6.3	3.8	7.8	69.2
SMa0852	*nodF*	613.5	n.a.	56.3	7.5	1.0	13.7	21.4
SMa0853	*nodE*	2177.1	n.a.	38.2	5.2	1.0	21.0	34.5
SMa0849	*syrM*	2477.6	n.a.	12.0	4.4	2.7	27.9	53.1
SMa0840	*nodD3*	498.2	n.a.	31.5	11.8	4.4	8.2	44.1
SMc02713	*rpoE3*	4166.7	n.a.	6.0	7.4	13.6	34.7	38.4
SMb20531	*rpoE7*	1350.2	n.a.	1.1	6.8	10.7	43.8	37.6
SMb20592	*rpoE8*	26 910.0	n.a.	8.0	7.8	7.4	32.1	44.7
SMb21484	*rpoE5*	1467.7	n.a.	15.1	32.3	7.2	13.0	32.5
SMb20030	*rpoE9*	1686.3	n.a.	16.4	14.0	24.7	16.8	28.0
SMc00646	*rpoH1*	27 997.4	n.a.	16.3	17.3	14.1	19.0	33.3
SMc03873	*rpoH2*	1588.7	n.a.	13.8	18.7	16.5	16.2	34.7

[a]The nodule/root expression ratio was determined using whole-organ Ribominus-like libraries (three biological repetitions).
Identifiers beginning with Mt and SM correspond to *M. truncatula* and *S. meliloti* genes, respectively.
RLK, receptor-like protein kinase; LRR, leucine-rich repeat; CR, cysteine-rich; AO, ascorbate oxidase; IZ, interzone; ZIII, zone III; VB, vascular bundles; FI, fraction I; FIId, distal fraction II; FIIp, proximal fraction II; n.a., not applicable.

which in turn activate the expression of genes important for nodule activity (Marino *et al.*, 2011). Consistently, RNA-seq data indicated that *MtRBOHA* was exclusively detected in the IZ and ZIII (Table 2), in contrast to other *MtRBOH* genes (Table S2).

On the bacterial side, expression of FixLJ-dependent genes was induced in the IZ or ZIII (clusters 6, 7, 9 and 12), which is consistent with the known response of this two-component regulator to low-oxygen conditions. Nevertheless, many FixLJ/oxygen-independent genes displayed similar expression patterns, indicating that additional transcription activators and signals are involved in triggering gene expression in nitrogen-fixing bacteroids. Several sigma factor-encoding genes were found upregulated at

the FIIp–IZ (*rpoE3*, *rpoE7*, *rpoE8*) and IZ–ZIII (*rpoE5*, *rpoE9*, *rpoH1*, *rpoH2*) transitions (Table 5) and may be among the actors participating in gene regulation in these regions. Reactive oxygen species are among the signals possibly involved in the regulation of gene expression at this stage. Indeed, the bacterial *katA* gene under the control of the H_2O_2-responsive regulator OxyR (Jamet *et al.*, 2005) was upregulated at the IZ, consistent with an increase in the H_2O_2 level at this stage. Also, a manganese transporter was upregulated in FIIP and the IZ, in agreement with the proposed role of manganese in the protection of *S. meliloti* against oxidative stress (Davies and Walker, 2007).

In addition to these genes, a series of nodule-preferential plant genes probably involved in signaling processes were identified, encoding receptors, protein kinases and calcium-signaling proteins, with for example 12 EF-hand proteins, all in the IZ and ZIII, among which were six calmodulins described to be symbiosome-associated (Liu *et al.*, 2006) (Tables 2 and 5, Figure 4). Corresponding signals remain to be identified, but these genes may represent important determinants for nodule-specific processes.

CONCLUSION

We describe here a resource that integrates highly sensitive and spatial information on plant and bacterial gene expression in indeterminate symbiotic nodules. The power of this approach was illustrated here notably with the study of the nodule meristem, a small region that is extremely difficult to analyze by whole-organ analysis, the localization of mRNAs strongly induced in nodules or the identification of candidate transcriptional and post-transcriptional regulators associated with different developmental transitions. Comprehensive data are thus made accessible to the community to address a wide range of questions and discover players in the plant and bacterial symbiotic programs. This is of obvious interest for both fundamental and applied biology, particularly at a time when programs aiming at transferring symbiotic nitrogen fixation to non-legume species are being implemented in different laboratories worldwide. It will be interesting in future studies to analyze the spatial expression pattern of transcript isoforms generated by differential splicing or alternative start/stop sites, as well as plant non-coding RNAs, which raise specific technical challenges for their identification and validation.

EXPERIMENTAL PROCEDURES

Plants and bacterial strains

Medicago truncatula cv. Jemalong A17 was grown in aeroponic caissons first for 18 days in medium supplemented with 10 mM NH_4NO_3 (Journet *et al.*, 2001), then for 4 days in nitrogen-free medium prior to inoculation with the *S. meliloti* 2011 strain GMI11495 (Sallet *et al.*, 2013). Root samples were harvested just before inoculation, following the nitrogen-starvation period. Nodules were harvested at 10 or 15 dpi for whole-organ or laser dissection analyses, respectively. Each biological repetition corresponded to an independent caisson (about 30 plants). For *lacZ* fusion analyses, plants were grown in tubes on nitrogen-depleted Fahraeus agar medium and inoculation was performed on 6-day-old seedlings (100 μl of a bacterial suspension at OD_{600} = 0.001).

Nodule inclusion, laser dissection and RNA extraction

After testing different fixation/inclusion conditions (see Methods S1), nodules were finally fixed in 100% methanol and included in Steedman's wax before sectioning using a rotary microtome (HM 355 Microm Thermoscientific, www.thermoscientific.fr). Nodule sections of 16 μm were stretched on PEN slides (Arcturus Bioscience, Excilone, www.excilone.com), each slide corresponding to 30–40 sections of a single nodule. Laser-capture microdissection was conducted with an Arcturus XT® microdissection system (Arcturus Bioscience), using 10 infrared and two ultraviolet pulses (50–100 nodules per biological repetition). The five nodule regions were dissected successively from the same nodule, all cells from the same region being pooled in a single CapSure Macro LCM (Arcturus Bioscience, Excilone). Cells were lysed immediately after dissection, using the PicoPure® RNA Isolation Kit (Arcturus Bioscience, Excilone) and stored at −20°C before RNA extraction. The quality and concentration of the RNA were evaluated with a Bioanalyser 2100 (Agilent Technologies, http://www.agilent.com/) on Agilent RNA Pico chips (see Figure S5 for a representative example). The RNA recovery was from 0.5–1 (FI) to 5–10 (ZIII) ng per nodule. Pooled RNAs were ethanol-precipitated.

For whole-organ analyses, total RNA was extracted with the *mir*Vana Isolation Kit (Ambion, Life Technologies, www.lifetechnologies.com/) using the total RNA isolation procedure. Residual contaminant DNA was removed with TURBO DNase (Ambion, Life Technologies). The RNA samples were then cleaned and concentrated using the SurePrep RNA purification kit (Fisher Bioblock Scientific, http://www.fishersci.com). The RNAs were quantified using a Nanodrop 1000 spectrophotometer (Thermo Fisher Scientific, http://www.nanodrop.com/) and their integrity was assessed using a Bioanalyzer (Agilent Technologies, http://www.home.agilent.com) [RNA integrity (RIN) number above 8 for roots].

Depletion of rRNA

For whole-organ analyses, oligocapture-based depletion or polyadenylated RNA extraction (Dynabeads) was carried out on 30 μg of total RNAs per sample.

For laser-dissected samples, oligonucleotide-based depletion was carried out on 40–100 ng total RNA per sample. Oligocaptures were performed with biotinylated, locked nucleic acid (LNA)-modified oligonucleotides (Sallet *et al.*, 2013). After ethanol precipitation, residual oligonucleotides were removed with Turbo DNAse (Ambion, Invitrogen) and RNA was purified on RNA Clean & Concentrator®-5 columns (Zymo Research, Proteigene, www.zymoresearch.com). Ribosomal-RNA depletion and RNA concentration were estimated on an Agilent RNA Pico chip.

In vitro RNA amplification

The RNA amplification was performed by *in vitro* transcription on rRNA-depleted RNA using the MessageAmp II Bacteria kit (Ambion) with an important modification, the use of Superscript III (Invitrogen) at 48°C. Amplified RNAs were purified with the SurePrep RNA Cleanup and Concentration Kit (Fisher Bioreagents, http://www.fishersci.com/), quantified with a Nanodrop and their profile analyzed on an Agilent RNA Nano chip (see Figure S5 for a representative example). About 3–10 μg of amplified RNAs was

obtained from 5 to 20 ng input rRNA-depleted RNA. One microgram of each sample was sent for RNA-sequencing.

Genome sequences, gene models and expression measurements

Oriented paired-end RNA sequencing (2 × 54 bases) was carried out by GATC Biotech AG, using an Illumina Hiseq 2000 platform (http://www.illumina.com/) as described (Parkhomchuk *et al.*, 2009). The RNA-seq data mapping was conducted on a virtual genome (available on the Symbimics website) composed of the genome of *S. meliloti* 2011 plus a new version of the *M. truncatula* A17 genome (Mt20120830-LIPM), annotated with EuGene and taking into account RNA-seq information generated in this project. Oriented transcript assemblies were obtained via an iterative process enabling the integration of velvet runs using various k-mer values (velvet release 1.2.03; parameters of assembly steps: -max_divergence 0.01 -read_trkg yes -exp_cov 100 -cov_cutoff 4 -long_mult_cutoff 0). The FASTA files of *S. meliloti* and *M. truncatula* transcripts deduced from annotation are available in the download section of our website (https://iant.toulouse.inra.fr/symbimics).

Read pairs were mapped using the GLINT software (T. Faraut and EC; http://lipm-bioinfo.toulouse.inra.fr/download/glint/) with parameters set as follows: matches ≥18 nucleotides, with ≤3 mismatches, no gap allowed, only best-scoring hits taken into account. Ambiguous matches (same best score) were removed. Pair counts were performed at the exon level taking into account the strand, and counts were then propagated at the level of corresponding transcripts.

Statistical and differential expression analyses

Normalization of raw counts was carried out with sets of libraries to be compared using the DESeq R package v. 1.12.0 (Anders and Huber, 2010). Estimation dispersion was calculated with the 'per-condition' method with the sharing Mode set to 'maximum'. Principal components analysis of normalized data was computed using the ade4 R package (Chessel *et al.*, 2004). Tests for differential expression were based on a model using the negative binomial distribution as described in the DESeq package. For each biological repetition, transcript relative abundance was estimated using the percentage of normalized counts in each fraction relative to the total number of normalized counts. The mean of the relative abundance per fraction was then calculated and their Euclidean distances computed with the hclust function from the stats R package (R Development Core Team, 2012). Clustering was computed with Ward's minimum variance method and a heat map generated with the gplots R package (2012) (http://CRAN.R-project.org/package=gplots).

In situ hybridization of mRNA and *lacZ* transcriptional fusion analyses

Fourteen-day-old nodules were fixed with formaldehyde, embedded in paraffin (Paraplast X-tra, Oxford Labware) and stored at 4°C until use. Nodule sections of 7 μm, generated using a rotating microtome, were put on Surgipath X-tra Adhesive micro slides (Leica, http://www.leica.com/), stretched on RNase-free water at 40°C, dried overnight at room temperature and stored at 4°C until use (for 2 weeks or less). The QuantiGene ViewRNA Assay was used with probe sets designed by Affymetrix from specific transcript regions (i.e. not showing strong similarities with notable transcripts from the same gene family) and according to the manufacturer's instructions. Slides were observed with a Zeiss Axioplan imaging microscope (http://www.zeiss.com/) either under bright field conditions or under fluorescence conditions with appropriate filter sets for Fast Red (ex: BP546/12, em: LP590) and Fast Blue (ex: BP620/60, em: BP700/75), and registered with an Axiocam MRC color camera (Zeiss) using AxioVision software.

To construct *lacZ* transcriptional fusions, the promoter regions of *S. meliloti visN* and SMc03023 were amplified by PCR using OCB1211-OCB1212 (OCB1211: CCATGGTACCGTTGTTTGCTGGTT CCGGAG; OCB1212: CTGCAGGACCGCGACATTTCCATGAC) and OCB1213-OCB1214 (OCB1213: CCATGGTACCTCATCGAGTTGGC CATGATG; OCB1214: ATGCATGCTGCCGATCTTCGACAG) as primers, respectively, then cloned in pGEM-T (Promega, http://www.promega.com/) and transferred as a *Nco*I–*Pst*I or *Nco*I–*Nsi*I fragment, respectively, in *Nco*I–*Nsi*I cut pCZ962 (del Giudice *et al.* 2011). The resulting plasmids were transferred from *Escherichia coli* to *S. meliloti* GMI11495 by triparental mating using pRK2013 (Figurski *et al.* 1979) as a helper. The *nodA* and *nodJ* fusions corresponded to the GMI 5801 and GMI 5873 strains (Maillet *et al.*, 1990). The *hemA:lacZ* fusion gene was carried on the pXLGD4 vector (Ardourel *et al.*, 1994) within GMI11495.

Bacterial *lacZ* transcriptional fusion expression in nodules was studied using β-galactosidase activity as a reporter, as described by Tian *et al.* (2012), with staining of 80 μm nodule sections.

ACKNOWLEDGEMENTS

This work was supported by the ANR grant 'SYMbiMICS' (ANR-08-GENO-106) and the French Laboratory of Excellence project 'TULIP' (ANR-10-LABX-41; ANR-11-IDEX-0002-02). We thank the FR AIB microscopy platform (Toulouse), notably Alain Jauneau and Yves Martinez, for providing us with the laser dissection equipment and excellent training, Agnès Lepage for her help with *lacZ* fusion analyses, Olivier Catrice and Marie-Christine Auriac (LIPM) for useful advice, and Jean-Marie Prosperi (INRA Montpellier) for providing us with *M. truncatula* seeds. Quantitative RT-PCR experiments were carried out at the Toulouse Genopole 'PLAGE' platform. The authors have no conflict of interest to declare.

SUPPORTING INFORMATION

Additional Supporting Information may be found in the online version of this article.

Figure S1. Comparison of polyA+ versus Ribominus-like transcript libraries

Figure S2. The RNA-seq read coverage for whole-nodule and laser-capture microdissection FIIp libraries

Figure S3. Scatter plot analyses of RNA-seq data generated from laser-dissected samples

Figure S4. Correlation circle resulting from principal component analysis of all laser-capture microdissection samples

Figure S5. Representative Bioanalyser (Agilent Pico chip) profile of a RNA sample (zone III sample) at different stages following laser-capture microdissection (1–2 ng aliquot).

Methods S1. Detailed procedures for laser-microdissection, RNA extraction and in vitro amplification.

Table S1. Correlation matrix for RNA-seq data.

Table S2a. The RNA-seq data for all *Medicago truncatula* mRNAs detected in root and nodule analyses (whole organs and laser-dissected samples, without systematic pair wise comparisons of laser-dissected samples).

Table S2b. Full RNA-seq data for all *Medicago truncatula* mRNAs detected in LCM samples (including systematic pair wise comparisons of all LCM fractions for each gene).

Table S3. List of *Medicago truncatula* mRNAs non represented by Affymetrix probes.
Table S4. The RNA-seq data for all *Sinorhizobium meliloti* transcripts (mRNAs and non-coding RNAs) detected in nodule analyses.
Table S5. Identification of differential Gene Ontology term distribution among *Medicago truncatula* and *Sinorhizobium meliloti* expression clusters.
Table S6. Nodule-preferential *Medicago truncatula* mRNAs found in expression clusters.
Table S7. The RNA-seq data for selected auxin and cytokinin-related genes.

REFERENCES

Anders, S. and Huber, W. (2010) Differential expression analysis for sequence count data. *Genome Biol.* **11**, R106.

Andrio, E., Marino, D., Marmeys, A., de Segonzac, M. D., Damiani, I., Genre, A., Huguet, S., Frendo, P., Puppo, A. and Pauly, N. (2013) Hydrogen peroxide-regulated genes in the *Medicago truncatula-Sinorhizobium meliloti* symbiosis. *New Phytol.* **198**, 179–189.

Ardourel, M., Demont, N., Debellé, F., Maillet, F., De Billy, F., Promé, J. C., Dénarié, J. and Truchet, G. (1994) *Rhizobium meliloti* lipooligosaccharide nodulation factors: different structural requirements for bacterial entry into target root hair cells and induction of plant symbiotic developmental responses. *Plant Cell*, **6**, 1357–1374.

Ariel, F., Brault-Hernandez, M., Laffont, C. *et al.* (2012) Two direct targets of cytokinin signaling regulate symbiotic nodulation in *Medicago truncatula*. *Plant Cell*, **24**, 3838–3852.

Barnett, M. J., Toman, C. J., Fisher, R. F. and Long, S. R. (2004) A dual-genome Symbiosis Chip for coordinate study of signal exchange and development in a prokaryote-host interaction. *Proc. Natl Acad. Sci. USA*, **101**, 16636–16641.

Benedito, V. A., Torres-Jerez, I., Murray, J. D. *et al.* (2008) A gene expression atlas of the model legume *Medicago truncatula*. *Plant J.* **55**, 504–513.

Boesten, B., Batut, J. and Boistard, P. (1998) DctBD-Dependent and -Independent expression of the *Sinorhizobium* (*Rhizobium*) *meliloti* C4-Dicarboxylate transport gene (dctA) during symbiosis. *Mol. Plant Microbe Interact.* **11**, 878–886.

Boscari, A., Del Giudice, J., Ferrarini, A., Venturini, L., Zaffini, A. L., Delledonne, M. and Puppo, A. (2013) Expression dynamics of the *Medicago truncatula* transcriptome during the symbiotic interaction with *Sinorhizobium meliloti*: which role for Nitric Oxide? *Plant Physiol.* **161**, 425–439.

Bourcy, M., Brocard, L., Pislariu, C. I., Cosson, V., Mergaert, P., Tadege, M., Mysore, K. S., Udvardi, M. K., Gourion, B. and Ratet, P. (2013) *Medicago truncatula* DNF2 is a PI-PLC-XD-containing protein required for bacteroid persistence and prevention of nodule early senescence and defense-like reactions. *New Phytol.* **197**, 1250–1261.

Boutilier, K., Offringa, R., Sharma, V. K. *et al.* (2002) Ectopic expression of *BABY BOOM* triggers a conversion from vegetative to embryonic growth. *Plant Cell*, **14**, 1737–1749.

Cam, Y., Pierre, O., Boncompagni, E., Hérouart, D., Meilhoc, E. and Bruand, C. (2012) Nitric oxide (NO): a key player in the senescence of *Medicago truncatula* root nodules. *New Phytol.* **196**, 548–560.

Capela, D., Filipe, C., Bobik, C., Batut, J. and Bruand, C. (2006) *Sinorhizobium meliloti* differentiation during symbiosis with alfalfa: a transcriptomic dissection. *Mol. Plant Microbe Interact.* **19**, 363–372.

Catalano, C. M., Lane, W. S. and Sherrier, D. J. (2004) Biochemical characterization of symbiosome membrane proteins from *Medicago truncatula* root nodules. *Electrophoresis*, **25**, 519–531.

Cebolla, A., Vinardell, J. M., Kiss, E., Olah, B., Roudier, F., Kondorosi, A. and Kondorosi, E. (1999) The mitotic inhibitor ccs52 is required for endoreduplication and ploidy-dependent cell enlargement in plants. *EMBO J.* **18**, 4476–4484.

Cerri, M. R., Frances, L., Laloum, T., Auriac, M. C., Niebel, A., Oldroyd, G. E., Barker, D. G., Fournier, J. and de Carvalho-Niebel, F. (2012) *Medicago truncatula* ERN transcription factors: regulatory interplay with NSP1/NSP2 GRAS factors and expression dynamics throughout rhizobial infection. *Plant Physiol.* **160**, 2155–2172.

Chessel, D., Dufour, A. B. and Thioulouse, J. (2004) The ade4 package - I: one-table methods. *R News*, **4**, 5–10.

Colebatch, G., Kloska, S., Trevaskis, B., Freund, S., Altmann, T. and Udvardi, M. K. (2002) Novel aspects of symbiotic nitrogen fixation uncovered by transcript profiling with cDNA arrays. *Mol. Plant Microbe Interact.* **15**, 411–420.

Colebatch, G., Desbrosses, G., Ott, T., Krusell, L., Montanari, O., Kloska, S., Kopka, J. and Udvardi, M. K. (2004) Global changes in transcription orchestrate metabolic differentiation during symbiotic nitrogen fixation in *Lotus japonicus*. *Plant J.* **39**, 487–512.

Combier, J. P., Frugier, F., de Billy, F. *et al.* (2006) MtHAP2-1 is a key transcriptional regulator of symbiotic nodule development regulated by microRNA169 in *Medicago truncatula*. *Genes Dev.* **20**, 3084–3088.

Coque, L., Neogi, P., Pislariu, C., Wilson, K. A., Catalano, C., Avadhani, M., Sherrier, D. J. and Dickstein, R. (2008) Transcription of *ENOD8* in *Medicago truncatula* nodules directs ENOD8 esterase to developing and mature symbiosomes. *Mol. Plant Microbe Interact.* **21**, 404–410.

Couzigou, J. M., Zhukov, V., Mondy, S. *et al.* (2012) *NODULE ROOT* and *COCHLEATA* maintain nodule development and are legume orthologs of *Arabidopsis BLADE-ON-PETIOLE* genes. *Plant Cell*, **24**, 4498–4510.

Czaja, L. F., Hogekamp, C., Lamm, P., Maillet, F., Martinez, E. A., Samain, E., Denarie, J., Kuster, H. and Hohnjec, N. (2012) Transcriptional responses toward diffusible signals from symbiotic microbes reveal MtNFP- and MtDMI3-dependent reprogramming of host gene expression by arbuscular mycorrhizal fungal lipochitooligosaccharides. *Plant Physiol.* **159**, 1671–1685.

Damiani, I., Baldacci-Cresp, F., Hopkins, J., Andrio, E., Balzergue, S., Lecomte, P., Puppo, A., Abad, P., Favery, B. and Hérouart, D. (2012) Plant genes involved in harbouring symbiotic rhizobia or pathogenic nematodes. *New Phytol.* **194**, 511–522.

Davies, B. W. and Walker, G. C. (2007) Disruption of *sitA* compromises *Sinorhizobium meliloti* for manganese uptake required for protection against oxidative stress. *J. Bacteriol.* **189**, 2101–2109.

Day, R. C., Grossniklaus, U. and Macknight, R. C. (2005) Be more specific! Laser-assisted microdissection of plant cells. *Trends Plant Sci.* **10**, 397–406.

del Giudice, J., Cam, Y., Damiani, I., Fung-Chat, F., Meilhoc, E., Bruand, C., Brouquisse, R., Puppo, A. and Boscari, A. (2011) Nitric oxide is required for an optimal establishment of the Medicago truncatula-Sinorhizobium meliloti symbiosis. *New Phytol.* **191**, 405–417.

D'Haeseleer, K., Den Herder, G., Laffont, C. *et al.* (2011). Transcriptional and post-transcriptional regulation of a NAC1 transcription factor in *Medicago truncatula* roots. *New Phytol.* **191**, 647–661.

El Yahyaoui, F., Kuster, H., Ben Amor, B. *et al.* (2004) Expression profiling in *Medicago truncatula* identifies more than 750 genes differentially expressed during nodulation, including many potential regulators of the symbiotic program. *Plant Physiol.* **136**, 3159–3176.

Fedorova, M., van de Mortel, J., Matsumoto, P. A., Cho, J., Town, C. D., VandenBosch, K. A., Gantt, J. S. and Vance, C. P. (2002) Genome-wide identification of nodule-specific transcripts in the model legume *Medicago truncatula*. *Plant Physiol.* **130**, 519–537.

Figurski, D.H., Meyer, R.J. and Helinski, D.R. (1979) Suppression of Co1E1 replication properties by the Inc P-1 plasmid RK2 in hybrid plasmids constructed in vitro. *J. Mol. Biol.* **133**, 295–318.

Frugier, F., Poirier, S., Satiat-Jeunemaitre, B., Kondorosi, A. and Crespi, M. (2000) A Kruppel-like zinc finger protein is involved in nitrogen-fixing root nodule organogenesis. *Genes Dev.* **14**, 475–482.

Galbraith, D. W. and Birnbaum, K. (2006) Global studies of cell type-specific gene expression in plants. *Annu. Rev. Plant Biol.* **57**, 451–475.

Gamas, P., de Billy, F. and Truchet, G. (1998) Symbiosis-specific expression of two *Medicago truncatula* nodulin genes, *MtN1* and *MtN13*, encoding products homologous to plant defense proteins. *Mol. Plant Microbe Interact.* **11**, 393–403.

Gaude, N., Bortfeld, S., Duensing, N., Lohse, M. and Krajinski, F. (2012) Arbuscule-containing and non-colonized cortical cells of mycorrhizal roots undergo extensive and specific reprogramming during arbuscular mycorrhizal development. *Plant J.* **69**, 510–528.

Godiard, L., Niebel, A., Micheli, F., Gouzy, J., Ott, T. and Gamas, P. (2007) Identification of new potential regulators of the *Medicago truncatula-Sinorhizobium meliloti* symbiosis using a large-scale suppression subtractive hybridization approach. *Mol. Plant Microbe Interact.* **20**, 321–332.

Godiard, L., Lepage, A., Moreau, S., Laporte, D., Verdenaud, M., Timmers, T. and Gamas, P. (2011) MtbHLH1, a bHLH transcription factor involved in *Medicago truncatula* nodule vascular patterning and nodule to plant metabolic exchanges. *New Phytol.* **191**, 391–404.

Gonzalez-Rizzo, S., Crespi, M. and Frugier, F. (2006) The *Medicago truncatula* CRE1 cytokinin receptor regulates lateral root development and early symbiotic interaction with *Sinorhizobium meliloti*. *Plant Cell*, **18**, 2680–2693.

Graham, M. A., Silverstein, K. A., Cannon, S. B. and VandenBosch, K. A. (2004) Computational identification and characterization of novel genes from legumes. *Plant Physiol.* **135**, 1179–1197.

Haag, A. F., Baloban, M., Sani, M. *et al.* (2011) Protection of *Sinorhizobium* against host cysteine-rich antimicrobial peptides is critical for symbiosis. *PLoS Biol.* **9**, e1001169.

Heckmann, A. B., Sandal, N., Bek, A. S., Madsen, L. H., Jurkiewicz, A., Nielsen, M. W., Tirichine, L. and Stougaard, J. (2011) Cytokinin induction of root nodule primordia in *Lotus japonicus* is regulated by a mechanism operating in the root cortex. *Mol. Plant Microbe Interact.* **24**, 1385–1395.

Hogekamp, C., Arndt, D., Pereira, P. A., Becker, J. D., Hohnjec, N. and Küster, H. (2011) Laser microdissection unravels cell-type-specific transcription in arbuscular mycorrhizal roots, including CAAT-box transcription factor gene expression correlating with fungal contact and spread. *Plant Physiol.* **157**, 2023–2043.

Hogslund, N., Radutoiu, S., Krusell, L. *et al.* (2009) Dissection of symbiosis and organ development by integrated transcriptome analysis of *Lotus japonicus* mutant and wild-type plants. *PLoS ONE*, **4**, e6556.

Hwang, I., Sheen, J. and Müller, B. (2012) Cytokinin signaling networks. *Annu. Rev. Plant Biol.* **63**, 353–380.

Jamet, A., Sigaud, S., Van de Sype, G., Puppo, A. and Herouart, D. (2003) Expression of the bacterial catalase genes during *Sinorhizobium meliloti-Medicago sativa* symbiosis and their crucial role during the infection process. *Mol. Plant Microbe Interact.* **16**, 217–225.

Jamet, A., Kiss, E., Batut, J., Puppo, A. and Herouart, D. (2005) The *katA* catalase gene is regulated by OxyR in both free-living and symbiotic *Sinorhizobium meliloti*. *J. Bacteriol.* **187**, 376–381.

Jeong, J., Suh, S., Guan, C., Tsay, Y. F., Moran, N., Oh, C. J., An, C. S., Demchenko, K. N., Pawlowski, K. and Lee, Y. (2004) A nodule-specific dicarboxylate transporter from alder is a member of the peptide transporter family. *Plant Physiol.* **134**, 969–978.

Jones, K. M., Kobayashi, H., Davies, B. W., Taga, M. E. and Walker, G. C. (2007) How rhizobial symbionts invade plants: the *Sinorhizobium-Medicago* model. *Nat. Rev. Microbiol.* **5**, 619–633.

Journet, E. P., El-Gachtouli, N., Vernoud, V., de Billy, F., Pichon, M., Dedieu, A., Arnould, C., Morandi, D., Barker, D. G. and Gianinazzi-Pearson, V. (2001) *Medicago truncatula ENOD11*: a novel RPRP-encoding early nodulin gene expressed during mycorrhization in arbuscule-containing cells. *Mol. Plant Microbe Interact.*, **14**, 737–748.

Kalo, P., Gleason, C., Edwards, A. *et al.* (2005) Nodulation signaling in legumes requires NSP2, a member of the GRAS family of transcriptional regulators. *Science*, **308**, 1786–1789.

Karunakaran, R., Ramachandran, V. K., Seaman, J. C., East, A. K., Mouhsine, B., Mauchline, T. H., Prell, J., Skeffington, A. and Poole, P. S. (2009) Transcriptomic analysis of *Rhizobium leguminosarum* biovar *viciae* in symbiosis with host plants *Pisum sativum* and *Vicia cracca*. *J. Bacteriol.* **191**, 4002–4014.

Kondorosi, E. and Kondorosi, A. (2004) Endoreduplication and activation of the anaphase-promoting complex during symbiotic cell development. *FEBS Lett.* **567**, 152–157.

Kouchi, H., Shimomura, K., Hata, S. *et al.* (2004) Large-scale analysis of gene expression profiles during early stages of root nodule formation in a model legume, *Lotus japonicus*. *DNA Res.* **11**, 263–274.

Krusell, L., Krause, K., Ott, T. *et al.* (2005) The sulfate transporter SST1 is crucial for symbiotic nitrogen fixation in *Lotus japonicus* root nodules. *Plant Cell*, **17**, 1625–1636.

Labes, M., Rastogi, V., Watson, R. and Finan, T. M. (1993) Symbiotic nitrogen fixation by a *nifA* deletion mutant of *Rhizobium meliloti*: the role of an unusual *ntrC* allele. *J. Bacteriol.* **175**, 2662–2673.

Laloum, T., De Mita, S., Gamas, P., Baudin, M. and Niebel, A. (2012) CCAAT-box binding transcription factors in plants: Y so many? *Trends Plant Sci.* **18**, 155–166.

Lefebvre, B., Timmers, T., Mbengue, M. *et al.* (2010) A remorin protein interacts with symbiotic receptors and regulates bacterial infection. *Proc. Natl Acad. Sci. USA*, **107**, 2343–2348.

Libault, M., Farmer, A., Joshi, T., Takahashi, K., Langley, R. J., Franklin, L. D., He, J., Xu, D., May, G. and Stacey, G. (2010) An integrated transcriptome atlas of the crop model *Glycine max*, and its use in comparative analyses in plants. *Plant J.* **63**, 86–99.

Limpens, E., Mirabella, R., Fedorova, E., Franken, C., Franssen, H., Bisseling, T. and Geurts, R. (2005) Formation of organelle-like N2-fixing symbiosomes in legume root nodules is controlled by DMI2. *Proc. Natl Acad. Sci. USA.* **102**, 10375–10380.

Limpens, E., Moling, S., Hooiveld, G., Pereira, P. A., Bisseling, T., Becker, J. D. and Küster, H. (2013) Cell- and tissue-specific transcriptome analyses of *Medicago truncatula* root nodules. *PLoS ONE*, **8**, e64377.

Liu, J., Miller, S. S., Graham, M. *et al.* (2006) Recruitment of novel calcium-binding proteins for root nodule symbiosis in *Medicago truncatula*. *Plant Physiol.* **141**, 167–177.

Lohar, D. P., Sharopova, N., Endre, G., Penuela, S., Samac, D., Town, C., Silverstein, K. A. and VandenBosch, K. A. (2006) Transcript analysis of early nodulation events in *Medicago truncatula*. *Plant Physiol.* **140**, 221–234.

Madsen, L. H., Tirichine, L., Jurkiewicz, A., Sullivan, J. T., Heckmann, A. B., Bek, A. S., Ronson, C. W., James, E. K. and Stougaard, J. (2010) The molecular network governing nodule organogenesis and infection in the model legume *Lotus japonicus*. *Nature Communications*, **12**, 1–10.

Maillet, F., Debellé, F. and Dénarié, J. (1990) Role of the *nodD* and *syrM* genes in the activation of the regulatory gene *nodD3*, and of the common and host-specific nod genes of *Rhizobium meliloti*. *Mol. Microbiol.* **4**, 1975–1984.

Mano, Y. and Nemoto, K. (2012) The pathway of auxin biosynthesis in plants. *J. Exp. Bot.* **63**, 2853–2872.

Marie, C., Plaskitt, K. A. and Downie, J. A. (1994) Abnormal bacteroid development in nodules induced by a glucosamine synthase mutant of *Rhizobium leguminosarum*. *Mol. Plant-Microbe Interact.* **7**, 482–487.

Marino, D., Andrio, E., Danchin, E. G., Oger, E., Gucciardo, S., Lambert, A., Puppo, A. and Pauly, N. (2011) A *Medicago truncatula* NADPH oxidase is involved in symbiotic nodule functioning. *New Phytol.* **189**, 580–592.

Marsh, J. F., Rakocevic, A., Mitra, R. M., Brocard, L., Sun, J., Eschstruth, A., Long, S. R., Schultze, M., Ratet, P. and Oldroyd, G. E. (2007) *Medicago truncatula* NIN is essential for rhizobial-independent nodule organogenesis induced by autoactive calcium/calmodulin-dependent protein kinase. *Plant Physiol.* **144**, 324–335.

Mathesius, U., Schlaman, H. R., Spaink, H., Sautter, C., Rolfe, B. G. and Djordjevic, M. A. (1998) Auxin transport inhibition precedes root nodule formation in white clover roots and is regulated by flavonoids and derivatives of chitin oligosaccharides. *Plant J.* **14**, 23–34.

Mathis, R., Grosjean, C., de Billy, F., Huguet, T. and Gamas, P. (1999) The early nodulin gene *MtN6* is a novel marker for events preceding infection of *Medicago truncatula* roots by *Sinorhizobium meliloti*. *Mol. Plant Microbe Interact.* **12**, 544–555.

Maunoury, N., Redondo-Nieto, M., Bourcy, M. *et al.* (2010) Differentiation of symbiotic cells and endosymbionts in *Medicago truncatula* nodulation are coupled to two transcriptome-switches. *PLoS ONE*, **5**, e9519.

Mbengue, M., Camut, S., de Carvalho-Niebel, F. *et al.* (2010) The *Medicago truncatula* E3 Ubiquitin Ligase PUB1 interacts with the LYK3 Symbiotic receptor and negatively regulates infection and nodulation. *Plant Cell*, **22**, 3474–3488.

Meilhoc, E., Cam, Y., Skapski, A. and Bruand, C. (2010) The response to nitric oxide of the nitrogen-fixing symbiont *Sinorhizobium meliloti*. *Mol. Plant Microbe Interact.* **23**, 748–759.

Mergaert, P., Nikovics, K., Kelemen, Z., Maunoury, N., Vaubert, D., Kondorosi, A. and Kondorosi, E. (2003) A novel family in *Medicago truncatula* consisting of more than 300 nodule-specific genes coding for small, secreted polypeptides with conserved cysteine motifs. *Plant Physiol.* **132**, 161–173.

Messinese, E., Mun, J. H., Yeun, L. H. *et al.* (2007) A novel nuclear protein interacts with the symbiotic DMI3 calcium- and calmodulin-dependent protein kinase of *Medicago truncatula*. *Mol. Plant Microbe Interact.* **20**, 912–921.

Middleton, P. H., Jakab, J., Penmetsa, R. V. *et al.* (2007) An ERF transcription factor in *Medicago truncatula* that is essential for Nod Factor signal transduction. *Plant Cell*, **19**, 1221–1234.

Mitra, R. M., Shaw, S. L. and Long, S. R. (2004) Six nonnodulating plant mutants defective for Nod factor-induced transcriptional changes associated with the legume-rhizobia symbiosis. *Proc. Natl Acad. Sci. USA*, **101**, 10217–10222.

Moreau, S., Verdenaud, M., Ott, T., Letort, S., de Billy, F., Niebel, A., Gouzy, J., de Carvalho-Niebel, F. and Gamas, P. (2011) Transcription reprogramming during root nodule development in *Medicago truncatula*. *PLoS ONE*, **6**, e16463.

Murray, J. D. (2011) Invasion by invitation: rhizobial infection in legumes. *Mol. Plant Microbe Interact.* **24**, 631–639.

Murray, J. D., Karas, B. J., Sato, S., Tabata, S., Amyot, L. and Szczyglowski, K. (2007) A cytokinin perception mutant colonized by *Rhizobium* in the absence of nodule organogenesis. *Science*, **315**, 101–104.

Okushima, Y., Fukaki, H., Onoda, M., Theologis, A. and Tasaka, M. (2007) ARF7 and ARF19 regulate lateral root formation via direct activation of LBD/ASL genes in *Arabidopsis*. *Plant Cell*, **19**, 118–130.

Oldroyd, G. E. and Long, S. R. (2003) Identification and characterization of *Nodulation-Signaling Pathway 2*, a gene of *Medicago truncatula* involved in Nod factor signaling. *Plant Physiol.* **131**, 1027–1032.

Oldroyd, G. E., Murray, J. D., Poole, P. S. and Downie, J. A. (2011) The rules of engagement in the legume-rhizobial symbiosis. *Annu. Rev. Genet.* **45**, 119–144.

Osipova, M. A., Mortier, V., Demchenko, K. N., Tsyganov, V. E., Tikhonovich, I. A., Lutova, L. A., Dolgikh, E. A. and Goormachtig, S. (2012) Wuschel-related homeobox5 gene expression and interaction of CLE peptides with components of the systemic control add two pieces to the puzzle of autoregulation of nodulation. *Plant Physiol.* **158**, 1329–1341.

Ott, T., van Dongen, J. T., Gunther, C., Krusell, L., Desbrosses, G., Vigeolas, H., Bock, V., Czechowski, T., Geigenberger, P. and Udvardi, M. K. (2005) Symbiotic leghemoglobins are crucial for nitrogen fixation in legume root nodules but not for general plant growth and development. *Curr. Biol.* **15**, 531–535.

Parkhomchuk, D., Borodina, T., Amstislavskiy, V., Banaru, M., Hallen, L., Krobitsch, S., Lehrach, H. and Soldatov, A. (2009) Transcriptome analysis by strand-specific sequencing of complementary DNA. *Nucleic Acids Res.* **37**, e123.

Pérez Guerra, J. C., Coussens, G., De Keyser, A., De Rycke, R., De Bodt, S., Van De Velde, W., Goormachtig, S. and Holsters, M. (2010) Comparison of developmental and stress-induced nodule senescence in *Medicago truncatula*. *Plant Physiol.* **152**, 1574–1584.

Petricka, J.J., Winter, C.M. and Benfey, P.N. (2012) Control of *Arabidopsis* Root Development. *Annu Rev Plant Biol.* **63**, 563–590.

Pislariu, C. I. and Dickstein, R. (2007) An IRE-like AGC kinase gene, *MtIRE*, has unique expression in the invasion zone of developing root nodules in *Medicago truncatula*. *Plant Physiol.* **144**, 682–694.

Plet, J., Wasson, A., Ariel, F., Le Signor, C., Baker, D., Mathesius, U., Crespi, M. and Frugier, F. (2011) MtCRE1-dependent cytokinin signaling integrates bacterial and plant cues to coordinate symbiotic nodule organogenesis in *Medicago truncatula*. *Plant J.* **65**, 622–633.

R Development Core Team (2012) *R: A Language and Environment for Statistical Computing*. Vienna, Austria: R Foundation for Statistical Computing.

Ramsay, K., Jones, M. G. and Wang, Z. (2006) Laser capture microdissection: a novel approach to microanalysis of plant-microbe interactions. *Mol. Plant Pathol.* **7**, 429–435.

Rogers, E. D., Jackson, T., Moussaieff, A., Aharoni, A. and Benfey, P. N. (2012) Cell type-specific transcriptional profiling: implications for metabolite profiling. *Plant J.* **70**, 5–17.

Rost, T. L. (2011) The organization of roots of dicotyledonous plants and the positions of control points. *Ann. Bot.* **107**, 1213–1222.

Roudier, F., Fedorova, E., Lebris, M., Lecomte, P., Gyorgyey, J., Vaubert, D., Horvath, G., Abad, P., Kondorosi, A. and Kondorosi, E. (2003) The *Medicago* species A2-type cyclin is auxin regulated and involved in meristem formation but dispensable for endoreduplication-associated developmental programs. *Plant Physiol.* **131**, 1091–1103.

Sallet, E., Roux, B., Sauviac, L. *et al.* (2013) Next-Generation annotation of prokaryotic genomes with EuGene-P: application to *Sinorhizobium meliloti* 2011. *DNA Res.* **20**, 339–354.

Schlaman, H. R., Horvath, B., Vijgenboom, E., Okker, R. J. and Lugtenberg, B. J. (1991) Suppression of nodulation gene expression in bacteroids of *Rhizobium leguminosarum* biovar *viciae*. *J. Bacteriol.* **173**, 4277–4287.

Schmid, M. W., Schmidt, A., Klostermeier, U. C., Barann, M., Rosenstiel, P. and Grossniklaus, U. (2012) A powerful method for transcriptional profiling of specific cell types in eukaryotes: laser-assisted microdissection and RNA sequencing. *PLoS ONE*, **7**, e29685.

Severin, A. J., Woody, J. L., Bolon, Y. T. *et al.* (2010) RNA-Seq Atlas of *Glycine max*: a guide to the soybean transcriptome. *BMC Plant Biol.* **10**, 160.

Sharma, S. B. and Signer, E. R. (1990) Temporal and spatial regulation of the symbiotic genes of *Rhizobium meliloti* in planta revealed by transposon Tn5-gusA. *Genes Dev.* **4**, 344–356.

Soupène, E., Foussard, M., Boistard, P., Truchet, G. and Batut, J. (1995) Oxygen as a key developmental regulator of *Rhizobium meliloti* N2-fixation gene expression within the alfalfa root nodule. *Proc. Natl Acad. Sci. USA*, **92**, 3759–3763.

Sourjik, V., Muschler, P., Scharf, B. and Schmitt, R. (2000) VisN and VisR are global regulators of chemotaxis, flagellar, and motility genes in Sinorhizobium (Rhizobium) meliloti. *J. Bacteriol.* **182**, 782–788.

Suzaki, T., Yano, K., Ito, M., Umehara, Y., Suganuma, N. and Kawaguchi, M. (2012) Positive and negative regulation of cortical cell division during root nodule development in *Lotus japonicus* is accompanied by auxin response. *Development*, **139**, 3997–4006.

Takanashi, K., Takahashi, H., Sakurai, N., Sugiyama, A., Suzuki, H., Shibata, D., Nakazono, M. and Yazaki, K. (2012) Tissue-specific transcriptome analysis in nodules of *Lotus japonicus*. *Mol. Plant Microbe Interact.* **25**, 869–876.

Tarayre, S., Vinardell, J. M., Cebolla, A., Kondorosi, A. and Kondorosi, E. (2004) Two classes of the CDh1-type activators of the anaphase-promoting complex in plants: novel functional domains and distinct regulation. *Plant Cell*, **16**, 422–434.

Tian, C. F., Garnerone, A. M., Mathieu-Demazière, C., Masson-Boivin, C. and Batut, J. (2012) Plant-activated bacterial receptor adenylate cyclases modulate epidermal infection in the *Sinorhizobium meliloti-Medicago* symbiosis. *Proc. Natl. Acad Sci. USA* **109**, 6751–6756.

Timmers, A.C., Soupene, E., Auriac, M.C., de Billy, F., Vasse, J., Boistard, P. and Truchet, G. (2000) Saprophytic intracellular rhizobia in alfalfa nodules. *Mol. Plant Microbe Interact.* **13**, 1204–1213.

Tirichine, L., Sandal, N., Madsen, L. H., Radutoiu, S., Albrektsen, A. S., Sato, S., Asamizu, E., Tabata, S. and Stougaard, J. (2007) A gain-of-function mutation in a cytokinin receptor triggers spontaneous root nodule organogenesis. *Science*, **315**, 104–107.

Udvardi, M. and Poole, P. (2013) Transport and metabolism in legume-rhizobia symbioses. *Annu. Rev. Plant Biol.* **64**, 29.21–29.25.

Van de Velde, W., Guerra, J. C., De Keyser, A., De Rycke, R., Rombauts, S., Maunoury, N., Mergaert, P., Kondorosi, E., Holsters, M. and Goormachtig, S. (2006) Aging in legume symbiosis. A molecular view on nodule senescence in *Medicago truncatula*. *Plant Physiol.* **141**, 711–720.

Van de Velde, W., Zehirov, G., Szatmari, A. *et al.* (2010) Plant peptides govern terminal differentiation of bacteria in symbiosis. *Science*, **327**, 1122–1126.

Vanstraelen, M., Baloban, M., Da Ines, O., Cultrone, A., Lammens, T., Boudolf, V., Brown, S. C., De Veylder, L., Mergaert, P. and Kondorosi, E. (2009) APC/C-CCS52A complexes control meristem maintenance in the *Arabidopsis* root. *Proc. Natl Acad. Sci. USA*, **106**, 11806–11811.

Vasse, J., de Billy, F., Camut, S. and Truchet, G. (1990) Correlation between ultrastructural differentiation of bacteroids and nitrogen fixation in alfalfa nodules. *J. Bacteriol.* **172**, 4295–4306.

Vernié, T., Moreau, S., de Billy, F., Plet, J., Combier, J. P., Rogers, C., Oldroyd, G., Frugier, F., Niebel, A. and Gamas, P. (2008) EFD is an ERF transcription factor involved in the control of nodule number and differentiation in *Medicago truncatula*. *Plant Cell*, **20**, 2696–2713.

Vernoud, V., Journet, E. and Barker, D. (1999) MtENOD20, a Nod factor-inducible molecular marker for root cortical cell activation. *Mol. Plant-Microbe. Interact.* **12**, 604–614.

Vinardell, J.M., Fedorova, E., Cebolla, A., Kevei, Z., Horvath, G., Kelemen, Z., Tarayre, S., Roudier, F., Mergaert, P., Kondorosi, A. and Kondorosi, E. (2003) Endoreduplication mediated by the anaphase-promoting complex activator CCS52A is required for symbiotic cell differentiation in *Medicago truncatula* nodules. *Plant Cell*, **15**, 2093–2105.

Wang, D., Griffitts, J., Starker, C., Fedorova, E., Limpens, E., Ivanov, S., Bisseling, T. and Long, S. (2010) A nodule-specific protein secretory pathway required for nitrogen-fixing symbiosis. *Science*, **327**, 1126–1129.

Young, N. D., Debellé, F., Oldroyd, G. E. *et al.* (2011) The *Medicago* genome provides insight into the evolution of rhizobial symbioses. *Nature*, **480**, 520–524.

de Zelicourt, A., Diet, A., Marion, J., Laffont, C., Ariel, F., Moison, M., Zahaf, O., Crespi, M., Gruber, V. and Frugier, F. (2012) Dual involvement of a *Medicago truncatula* NAC transcription factor in root abiotic stress response and symbiotic nodule senescence. *Plant J.* **70**, 220–230.

Zhang, X. W., Jia, L. J., Zhang, Y., Jiang, G., Li, X., Zhang, D. and Tang, W. H. (2012) *In planta* stage-specific fungal gene profiling elucidates the molecular strategies of *Fusarium graminearum* growing inside wheat coleoptiles. *Plant Cell*, **24**, 5159–5176.

